Clays and Clay Minerals (2024), **72**, e14, 1–18
doi:10.1017/cmn.2024.21

Original Paper

Mobility patterns of rare earth elements in diagenetically altered vitric tuff shaped by illite-smectite

Branimir Šegvić[1], Luka Badurina[1,2], Adriano E. Braga[3], Oleg Mandic[4], Kevin Werts[1], Emily Doyle[1], Damir Slovenec[5], Frane Marković[6], Goran Slivšek[7] and Vedad Demir[8]

[1]Texas Tech University, Department of Geosciences, Lubbock, TX 79409, USA; [2]CTLGroup, Mount Prospect, IL 60056, USA; [3]Purdue University, Davidson School of Chemical Engineering, West Lafayette, IN 47907, USA; [4]Naturhistorisches Museum Wien, Geological-Paleontological Department, Burgring 7, 1010 Vienna, Austria; [5]Croatian Geological Survey, Sachsova 2, 10000 Zagreb, Croatia; [6]University of Zagreb, Faculty of Science, Department of Geology, Horvatovac 102b, 10000 Zagreb, Croatia; [7]Institute for Anthropological Research, Centre for Applied Bioanthropology, Gajeva ulica 32, 10000 Zagreb, Croatia and [8]Geological Survey of Federation of Bosnia and Herzegovina, Ustanička 11, 71210 Sarajevo-Ilidža, Bosnia and Herzegovina

Abstract

The mobility of rare-earth elements (REE) in low-grade diagenetic regimes, potentially leading to their clay-mediated fractionation, remains poorly understood. This study draws evidence from the argillitized Miocene tuff of the Southwestern Pannonian Basin (SPB) and adjacent Dinarides intramontane basins (DIB) to investigate the role of illite-smectite (I-S) in controlling early diagenetic REE behavior. The present research relies on detailed mineralogical, geochemical, and gas adsorption characterization of altered tuff, focusing on comparative analyses of the REE chemistry obtained by *in situ* laser ablation inductively coupled plasma mass spectrometry of glass shards and that of spatially related authigenic clay minerals. The depositional environment, in which the volcanic glass alteration took place, gave rise to the composition of secondary paragenesis, revealing a dominance of I-S. The normalized REE geochemistry of clay separates show similarities to unaltered glass, but notable differences indicate fluctuations in fluid/rock ratio environments. The redox conditions during glass alteration are reflected in Ce and Eu anomalies and indicate the ranges from oxic to anoxic across the analyzed tuffs. The results showed that I-S, formed through volcanic glass diagenesis, inherits magmatic REE signatures but also fractionates REE based on more reducing physiochemical conditions. The strong correlation between smectite content of I-S and a total budget of fractionated REE posits the smectite interlayers as prime factors controlling the REE fractionation during volcanic ash diagenesis. Furthermore, greater specific surface area values and development of slit-shaped porosity along the non-basal edges of I-S particles contributed to REE adsorption. These findings contribute to our understanding of REE behavior in low-temperature diagenetic environments, emphasizing the significance of clay minerals in retaining and fractionating these elements which may lead ultimately to the formation of economically viable ion-adsorption clay deposits.

Keywords: clay adsorption; Dinarides intramontane basins; illite-smectite; rare-earth elements (REE) mobility; tuff diagenesis

(Received: 26 February 2024; revised: 17 April 2024; accepted: 07 May 2024)

Introduction

Fifteen lanthanides, along with Sc and Y, make up a group of rare-earth elements (REE). These lithophile elements are predominantly trivalent, electropositive, and possess refractory properties (McLennan, 1994; Taylor and McLennan, 1995). The orbital configuration of REE gives rise to their remarkably similar physical and chemical properties where subtle differences in chemical behavior arise from their systematic variations in ionic radii and complexations, as well as the distinct redox states of Ce and Eu (Dubinin, 2004; Willis and Johannesson, 2011; McLennan and Ross Taylor, 2012). From an application perspective, REE play a key role in the advancement of new technologies and the transition to a green, low-carbon economy (Binnemans et al., 2013; Balaram, 2019). As these technologies gain broader acceptance, the demand for REE is expected to rise (Alonso et al., 2012; Gismondi et al., 2022). Contrary to their name, REE are not truly rare. They are, on average, as abundant as Cu or Ni in the Earth's crust (Sekine, 1963; Ronov and Yaroshevsky, 1969). However, unlike the two metals, REE are not found in concentrated deposits, making their extraction more challenging (Gupta and Krishnamurthy, 1992; Humphries, 2010).

Contrary to high-temperature geologic environments, the comportment of REE in low-grade regimes is still poorly understood (Cornu et al., 2005; Laveuf and Cornu, 2009; Zhang et al., 2014; Badurina and Šegvić, 2022). Their solubility, however, is found to increase generally during weathering and diagenesis (Burkov and Podporina, 1967; Elliott, 2020). The complexing

Corresponding author: Branimir Šegvić; Email: Branimir.Segvic@ttu.edu
Cite this article: Šegvić B., Badurina L., Braga A.E., Mandic O., Werts K., Doyle E., Slovenec D., Marković F., Slivšek G., & Demir V. (2024). Mobility patterns of rare earth elements in diagenetically altered vitric tuff shaped by illite-smectite. *Clays and Clay Minerals* **72**, e14, 1–18. https://doi.org/10.1017/cmn.2024.21

ability of REE by inorganic and organic ligands at near-surface aqueous conditions tends to increase from light to heavy lanthanides (Topp, 1965), aligning with the trend of their solubility increasing as ionic radii decrease (Martin et al., 1976). This relates to the linear relationship between the relative ionic potential of REE and their enthalpy of hydration (Dileep Kumar, 1984). Once released from their primary source, REE precipitate readily in secondary phases (e.g. decrespignyite-(Y), paratooite-(La), Mn minerals; Brugger et al., 2006; Berti et al., 2022; Berti et al., 2023) or get ion-sorbed by clay minerals, such as kaolinite (Cheshire et al., 2018; Ercan et al., 2022; Ou et al., 2022), halloysite (Li and Zhou, 2020), and various 2:1 clay minerals (Liu et al., 2019; Borst et al., 2020; Li and Zhou, 2020; Luo et al., 2023; Wu et al., 2023). Although the specific nature of the chemical bonds between REE and the clay structure is still unknown, it has been observed that REE tend to be adsorbed weakly on broken edge sites of clay minerals and charged aluminol or siloxane surfaces through the processes of ion exchange and surface complexation. These mechanisms may result ultimately in REE fractionation and enrichment (Hao et al., 2019; Zhou et al., 2020; Schroeder et al., 2022; Wu et al., 2023; Zhao et al., 2023). Recent research has also reported that certain bacteria found in the diagenetic environment may secrete low molecular weight organic compounds known as metallophores. These compounds exhibit high selectivity and affinity for lanthanides (Zytnick et al., 2023). The lanthanophore may therefore be used for recovery of REE (Pol et al., 2014; Daumann et al., 2022); however, the relationship between the REE-bearing bacteria and clay minerals remains largely unknown (Neubauer et al., 2000).

The Carpathian-Pannonian Region (CPR) of central Europe experienced a significant extension of the continental lithosphere during the Miocene, which led to the most intense volcanic activity in Europe at the time (Szabó et al., 1992; Németh et al., 2001; Roşu et al., 2004; Kovács et al., 2007; Harangi et al., 2015). As a result, large amounts of felsic to intermediate tephra covered areas of the Southwestern Pannonian Basin (SPB) (Mandic et al., 2012; Rybár et al., 2019; Gverić et al., 2020; Marković et al., 2021; Grizelj et al., 2023; Šegvić et al., 2023a) and adjacent Dinarides intramontane basins (DIB) (Krstić et al., 2001; Mandic et al., 2009; Šegvić et al., 2014; Badurina et al., 2021) (Fig. 1). There, with prolonged weathering, the pyroclastic material altered into clay-rich assemblages (Grizelj et al., 2023; Šegvić et al., 2023a). To assess the potential for REE retention in argillaceous tuffs, understanding the post-emplacement trajectories of trace elements in different

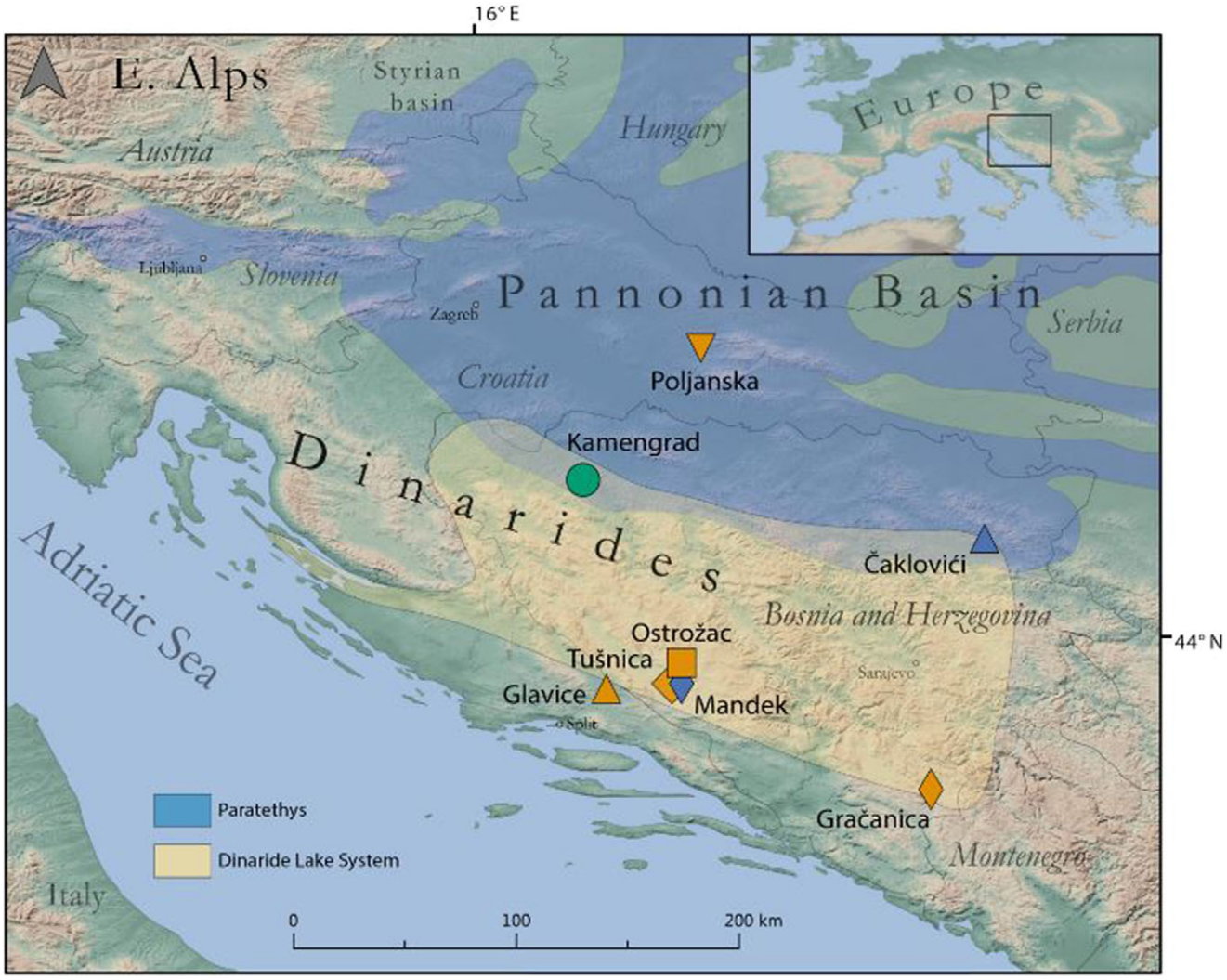

Figure 1. Geographical map of the sampling localities.

https://doi.org/10.1017/cmn.2024.21 Published online by Cambridge University Press

geological environments is crucial. This issue has been addressed in various studies through the analysis of fresh glass and its alteration products which were sampled from diverse locations (Christidis, 1998; McHenry, 2009; Kiipli et al., 2017). This required considerable amounts of analyzed material susceptible to potential contamination from allochthonous detritus. In this research, however, the novel method which examines the spatially associated fresh volcanic material and associated clay minerals to reconstruct REE mobility in a low-grade diagenetic environment was utilized (Badurina and Šegvić, 2022). Put differently, this study relies on comparing the REE chemistry collected by *in situ* laser ablation inductively coupled plasma mass spectrometry (LA-ICP-MS) of glass shards with that of genetically related illite-smectite gathered in the form of fraction separates. This study examines nine altered Miocene tuffs from two SPB and four DIB basins which are marked by diverse basinal stratigraphy (Fig. 1; Table 1). The aim of this contribution is to bring further insights to the following research questions: (i) to what extent does the morphology, geochemistry, and mineralogy of clay alteration products impact REE mobility?, (ii) how does the depositional environment conditions of airborne distal tephra influence the REE fractionation and retention during weathering?, and (iii) could eogenetic clays formed on a tuffaceous substrate serve as a potential regolith-hosted REE deposit?

Geological background

The Alpine-Carpathian-Dinarides orogenic system and the Pannonian Basin System (PBS) are two of the most important geological features in central and southeastern Europe. The PBS is a wide back-arc extensional basin, floored by a thin continental lithosphere, which was formed as a result of the northward drift and the indentation of the Adriatic promontory (Roeder and Bachmann, 1996; Schmid et al., 2004; Schmid et al., 2008), the rotation of the Tiszia terrane (Balla, 1986; Csontos et al., 1992; Bada and Horváth, 2001; Csontos and Vörös, 2004) and their subsequent collision with the European margin (Schmid et al., 2008; Schmid et al., 2020). Ultimately, the formation of PBS was caused by the eastward extension of an Alpine orogenic wedge and Tiszia toward the eastern Carpathians. This was a consequence of the subduction roll-back of the lithosphere of the Carpathian flysch basin (Horváth, 1995; Bada and Horváth, 2001; Horváth et al., 2006; Šujan et al., 2021). During the Early and Middle Miocene, the climate in the southern PBS area experienced warming, accompanied by contrasting humidity conditions along the Dinarides transection: humid toward the sea and arid inland (Andrić-Tomašević et al., 2021; Pavelić et al., 2022). Additionally, the synrift in the Southern Pannonian Basin and the related extension in the Dinarides reactivated reversed Paleogene faults, providing necessary depositional space (de Leeuw et al., 2012; Pavelić and Kovačić, 2018; van Unen et al., 2019). Furthermore, the Middle Miocene time saw an initial transgression and subsequent sea level change of the Paratethys Sea in the southern Pannonian Basin (Mandic et al., 2019a; Mandic et al., 2019b; Mandic et al., 2019c). These climatic, tectonic, and eustatic changes resulted in diverse depositional environments ranging from lacustrine to marine settings, creating a dynamic geological landscape (Pavelić et al., 2003; Piller et al., 2007; Bakrač et al., 2010; Holbourn et al., 2015; Pavelić and Kovačić, 2018; Mandic et al., 2019a; Mandic et al., 2019b; Grizelj et al., 2020; Pavelić et al., 2022; Hajek-Tadesse et al., 2023; Matošević et al., 2023). The tectonic evolution of PBS was characterized by extensive volcanic activity, which produced large amounts of felsic or intermediate pyroclastic material (Harangi and Lenkey, 2007; Seghedi and Downes, 2011; Lukács et al., 2018) now found in the form of intercalated tephra layers within the PBS clastic strata (Pavelić and Kovačić, 2018; Gverić et al., 2020; Grizelj et al., 2023; Šegvić *et al.*, 2023a).

The Dinarides are part of the Alpine-Himalayan Orogeny, which experienced a significant uplift during the Middle Eocene and Early Oligocene (Pamić et al., 1998; Tari, 2002; Pamić and Hrvatović 2003). Following this orogenic phase, extensional tectonics prevailed in the Late Oligocene as a result of the rifting

Table 1. List of analyzed altered tuff from DIB and SPB

Sample	Basin	Age (Ma)	Petrographic description	Thickness (m)	Depositional setting	Location (WGS84)	Reference
Gračanica	Gacko (DIB)	15.31±0.16 (Ar–Ar)	Altered vitroclastic tuff	1	Lacustrine	E18.47944; N43.17751	Mandic et al. (2011)
Kamengrad 2.4	Kamengrad (DIB)	~18–15 (stratigraphy)	Altered vitroclastic tuff	0.6	Lacustrine	E16.528423; N44.806434	Sunarić et al. (1976)
Kamengrad 2.63	Kamengrad (DIB)	~18–15 (stratigraphy)	Vitroclastic tuff	2	Lacustrine	E16.527853; N44.806614	Sunarić et al. (1976)
Čaklovići	Tuzla (SPB)	~16.5	Altered vitroclastic tuff	3	Lacustrine to marine	E18.75055; N44.50884	Ćorić et al. (2018)
Glavice	Sinj (DIB)	17.3±0.03 (Ar–Ar)	Altered vitroclastic tuff	0.2	Lacustrine	E16.660667; N43.716583	Brlek et al. (2023)
Poljanska	North Croatian (SPB)	~17.2–16 (stratigraphy)	Altered vitroclastic tuff	0.3	Salina lake	E17.569; N45.453,	Pavelić et al. (2022)
Tušnica	Livno-Tomislavgrad (DIB)	17.00±0.17 (Ar–Ar)	Altered vitroclastic tuff	0.2	Lacustrine	E17.09194; N43.73996	de Leeuw et al. (2011)
Mandek	Livno-Tomislavgrad (DIB)	14.68±0.16 (Ar–Ar)	Vitroclastic tuff	6	Lacustrine	E17.02255; N43.73045	de Leeuw et al. (2011)
Ostrožac	Livno-Tomislavgrad (DIB)	~ 14.4 (magneto–stratigraphy)	Altered carbonate tuff	0.5	Lacustrine	E17.184953; N43.716136	de Leeuw et al. (2011)

DIB = Dinarides intramontane basins; SPB = Southern Pannonian Basin.

https://doi.org/10.1017/cmn.2024.21 Published online by Cambridge University Press

in the Pannonian Basin (Matenco and Radivojević, 2012; Andrić et al., 2017; Stojadinovic et al., 2017). This led to the formation of numerous NW-SE-trending Dinaride Intramontane Basins (DIB; de Leeuw et al., 2012; van Unen et al., 2019). The Miocene climatic optimum, characterized by a phase of persistent humidity, probably contributed to the development of stable, long-lived lake conditions in the Intramountainous Basins of the Dinarides (Zachos et al., 2001; Jiménez-Moreno et al., 2008). The DIB stratigraphic record, similar to that of the SPB, bears evidence of Miocene volcanism in the Pannonian Basin Region, manifested through numerous tuff layers documented throughout DIB (Mandic et al., 2009; Šegvić et al., 2014; Badurina et al., 2021).

The SPB and DIB distal tephra layers, depending on prevailing depositional conditions, are normally found altered into secondary hydrous minerals like clay minerals and zeolite (Gverić et al., 2020; Andrić-Tomašević et al., 2021; Badurina et al., 2021; Simić et al., 2021; Šegvić et al., 2023a). The formation of clay minerals from pyroclastic substrate typically requires prolonged periods of warm and hydrolyzing conditions (McHenry, 2009; Cunningham et al., 2016; Hong et al., 2017) and is influenced by paleoclimatic and paleoenvironmental constraints (Huff et al., 1998; Christidis and Huff, 2009; Huff, 2016). The SPB and DIB tuffaceous clays chosen for this study (Table 1) reflect long and stable weathering periods and typically consist of illite, smectite, and mixed-layer illite-smectite (Šegvić et al., 2014; Gverić et al., 2020; Badurina et al., 2021).

Materials and methods

Materials

Nine samples of altered tuff were selected for this study. They originate from eight SPB and DIB locations stretching from the North Croatian Basin (the area of Mt Papuk) of Eastern Croatia through the Tuzla, the Kamengrad, the Livno and the Gacko Basins of northern, western, and south Bosnia and Herzegovina, to the Sinj Basin in Dalmatia, southern Croatia (Fig. 1). The petrographic description, thickness, published age, depositional setting, and GPS coordinates are provided for each analyzed sample (Table 1).

The tuff from the North Croatian Basin was acquired from the section exposed at the Poljanska quarry of Mt Papuk (Pavelić et al., 2022). The Miocene depositional environment at the time of tuff deposition corresponded to a hydrologically closed salina lake (Šćavničar et al., 1983; Pavelić and Kovačić, 1999; Mandic et al., 2012; Pavelić and Kovačić, 2018). The felsic rhyolitic tuff at the base of the section is likely to be of Lower (to Middle) Miocene age and corresponds to similar occurrences found in Austria (Roetzel et al., 2014), Hungary (Pálfy et al., 2007), and Slovakia (Šarinová et al., 2021). The Poljanska quarry tuff consists of multiple beds, varying from 5 to 30 cm in thickness, intercalated with marls and dolomite (Pavelić et al., 2022).

Further to the south is the Tuzla Basin where the tuff was sampled at the Čaklovići locality about 7 km SSE of the city of Tuzla (Badurina et al., 2021). The lithified dark grey tuff exposure there is ~3 m thick and forms the base of ~30 m thick Middle Miocene costal and deltaic lacustrine sediment overlain by the Badenian marine shallow-water massive marl (Ćorić et al., 2018).

To the west, two tuff samples were taken from the Kamengrad Basin the deposits of which may be correlated with the main evolutionary phase (18–15 Ma) of the Dinarides Lake System (Kochansky-Devidé and Slišković, 1978; de Leeuw et al., 2012). The basinal infill is 2 km thick, with coal layers dominating the lower portion and limestone and marl in the upper portion (Sunarić et al., 1976). Both tuff samples were collected along the road from the closed Gornji Kamengrad coal mine to Okreč and are part of the limestone and marl dominated succession. The first tuff (2–40) was taken from a 60 cm thick light gray layer distinguished by the presence of dark minerals. The second tuff (2–63) was obtained from a 2 m thick, light gray, and laminated/banded layer, which does not contain any dark minerals.

At the south of Bosnia and Herzegovina the tuff samples were acquired from the Gacko and Livno-Tomislavgrad Basins. The tuff from the Gacko Basin was obtained at the Gračanica locality, specifically from the uppermost part of a lacustrine succession exposed in a large active coal pit in the southwest region of the Gacko Basin. Sampling focused on the lowermost 20 cm of a 1 m thick tuff layer. The section description showing the stratigraphic position of the tephra layer can be found in Mandic et al. (2011). $^{40}Ar/^{39}Ar$ measurements of feldspar separates revealed an age of 15.31±0.16 Ma.

Three tuff samples from three sections were recovered from the Livno-Tomislavgrad Basin. All sections were described and two were radiometrically dated by de Leeuw et al. (2011). The older tuff, which dates to ~17 Ma, is situated in the Tušnica section. It consists of a laterally continuous bed, ~20 cm thick, exhibiting a gray to white coloration. The tuff is notably enriched with flakes of dark mica and is found in a distinct and sharp contact with the surrounding coal seam. The younger tuff, with an age of ~14.68 Ma, was collected from the Lake Mandek locality. A discrete layer of volcanic ash there is 6 m thick and displays a whitish color and weak lithification. The lower part of the tuff's lithology remains uncertain due to dense vegetation covering the area. However, at the upper boundary, it transitions into lacustrine carbonates. The third tuff was collected in the upper part of the Ostrožac section at 762 m height. Its magnetostratigraphic age was estimated to be ~14.4 Ma (Table 1; de Leeuw et al., 2011). This tuff layer has a thickness of 50 cm and is found intercalated within lacustrine limestone.

Finally, the sample of tuff from the Sinj Basin was taken from the Glavice composite section and was dated to 17.295±0.028 Ma (Brlek et al., 2023). This vitroclastic to altered vitroclastic tuff is intercalated within the coal bearing lacustrine carbonates (Vranjković, 2011) emerging in the form of a massive, homogenous, tabular, plastic to compact layer with sharp top and bottom contacts (Šegvić et al., 2014).

Methods

X-ray diffraction (XRD) measurements were carried out at the Texas Tech Department of Geosciences using a Phillips X'Pert Pro PW3040 diffractometer equipped with a variable divergence slit set to 16 mm exposure area, 15 mm incident beam mask, and 0.04 radian primary and secondary soller slits. For semi-quantitative XRD analysis, 3 g of sample material was weighed. The selected material was later combined with 1 g (20 wt.%) of corundum powder and then milled using a McCrone mill. Samples were gently backloaded into a sample holder of 27 mm internal diameter. Global sample measurements were conducted on a rotating sample holder (8 rpm) using continuous scanning mode in the Bragg-Brentano geometry with CuKα radiation (40 kV and 40 mA). The step size was set at 0.026°2θ in a 5 to 64°2θ range with a total measurement time of 62 min. Measurements of oriented clay fractions were carried out using the same parameters in a 5 to 33°2θ range, with a total measurement time of 23 min. Oriented clay mounts were produced by dispersing crushed material in an ultrasonic bath, followed by the sedimentation of the clay fraction (<2 μm) using centrifugation (Šegvić et al., 2020). Subsequently, the specimens underwent treatment with ethylene glycol, and when

https://doi.org/10.1017/cmn.2024.21 Published online by Cambridge University Press

necessary, subjected to heating at 400 and 500°C. The present phases were discerned utilizing the PDF 4+ database in conjunction with the Bruker DIFFRAC.EVA software suite. Clay mineral diffraction traces were analyzed following the guidelines provided by Moore and Reynolds (1997) and Środoń (2013).

XRD traces were modelled using Sybilla© software, which integrated the formalism of Drits and Sakharov (1976). The fitting of diffraction patterns relies on a trial-and-error procedure, yielding optimal clay mineral structural and probability parameters to achieve the best fits with minimal differences between experimental and calculated patterns. This process also ensures the alignment of intensities of 00*l* reflections for each of the present clay phases. The number, nature, and stacking sequence of various compositional layers in mixed-layer minerals were considered as adjustable parameters (Uzarowicz et al., 2012; Šegvić et al., 2020). To produce experimental diffraction patterns, a single discrete clay mineral phase, namely illite, was introduced. Additionally, three disordered mixed-layer illite-smectite (I-S) phases (R0 I-S, R0 I-SS, R0 I-SSS) and one ordered mixed-layer illite-smectite phase (R1 I-SSS) were included. The second and third smectite in the I-S labeling signify different types of smectite components, distinguished from the preceding one by variations in water content and consequently, the *d*-spacing. In simpler terms, the expandable layers in I-S are bi-hydrated, in I-SS they are mono- and bi-hydrated, and in I-SSS, there can be up to three layers of water in the smectite component (Ferrage et al., 2007). Finally, a disordered kaolinite-smectite (K-S) phase (R0 K-S) was introduced to accommodate the presence of kaolinite in one of the analyzed samples. The semi-quantification of phyllosilicates in the separated clay fractions was carried out using the Sybilla© quantification algorithm.

The BGMN program was employed for Rietveld refinement through the Profex graphical user interface (Doebelin and Kleeberg, 2015). The structural parameters of analyzed phases were sourced from the Crystallography Open Database (COD) (Vaitkus et al., 2021) and the BGMN structure file repository (Doebelin and Kleeberg, 2015). For every identified phase, lattice parameters, peak-broadening parameters, and, if necessary, preferred orientation were refined, ensuring that they fell within physically acceptable ranges. Corundum served as an internal standard to assess the proportion of amorphous matter, including volcanic glass, in all analyzed sample (Dapiaggi et al., 2015).

Tuff samples rich in glass shards were prepared in the form of thick (~100 μm) sections and analyzed using LA-ICP-MS at Texas Tech University's GeoAnalytical Laboratory using an Agilent 7500cs quadrupole mass spectrometer equipped with a New Wave Resolution 213 nm solid state laser with dual-volume cell. The laser was operated at a spot size of 100 μm and a measured fluence of between 6 and 7 J cm^{-2} with a frequency of 10 Hz. The NIST-610 glass was utilized as the calibration standard while Si served as the internal standard element (Jochum et al., 2005). The glass shards were measured from the thin sections whereas the clay fractions from the studied samples were separated using centrifugation (Badurina and Šegvić, 2022) and then investigated using an LA-ICP-MS line raster analysis which has been shown to be adequate for the analysis of an inherently heterogeneous clayey material (Vannoorenberghe et al., 2020). Careful polishing of thin sections ensured the removal of potentially altered shard surfaces containing micro- or nano-sized clay inclusions. The time-resolved signal from LA-ICP-MS was examined to detect potential contamination. The precision and accuracy of the method were assessed using secondary standards USGS BHVO-2 G, RGM-1 and NIST-614 (Hollocher and Ruiz, 1995; Jochum et al., 2005; Schudel et al., 2015) (see Table S1 in the Supplementary material). To inspect trace element mobility during the alteration of volcanic glass, the glass and clay REE abundances were firstly normalized to Al_2O_3 concentrations of the respective samples (Gifkins and Allen, 2001). Such normalized values were than compared against each other using the equation of Nesbitt (1979).

The measurements of the specific surface area (SSA) of clay minerals have been utilized commonly to assess quantitatively their reactive surface sites to predict the sorption and mineral dissolution process in clay-rich sedimentary rocks and soils (Sanders et al., 2010; Macht et al., 2011). Consequently, higher SSA values of clay minerals were shown to be positively correlated with an increasing REE adsorption potential (Yang et al., 2019; Xu et al., 2020). Obtaining the SSA values involves measuring the adsorption of gaseous nitrogen by the material at its boiling point temperature. The adsorption isotherm is further fitted to the Brunauer–Emmett–Teller (BET) equation. This is the widely accepted technique for determining SSA values of phyllosilicates (Brigatti et al., 2013). BET measurements were completed at Purdue Catalysis Center at Purdue University. Prior to the N_2-physisorption experiments, 30–40 mg of powdered samples (US Standard No. 120, <125 μm) were firstly outgassed for 9 h at 120°C under vacuum ($<6\times10^{-3}$ mbar) to remove moisture and volatile organic compounds adsorbed to the material. The samples were then transferred to the measurement port attached to a gas/vacuum manifold. N_2-physisorption isotherms were acquired by dosing nitrogen at N_2 boiling temperature (77K, 196°C), using an adapted protocol issued by the American Society for Testing and Materials (ASTM, D4365-95, 2008). N_2-physisorption isotherms were acquired using a Micromeritics 3-Flex instrument. The surface area values were calculated following the BET equation (Brunauer et al., 1938). The average pore size and pore volume were obtained by fitting the N_2 desorption branch to the Barrett–Joyner–Halenda (BJH) equation (Barrett et al., 1951). The precision defined by the standard deviation of five repeated analyses was in the range of 2–7%.

Results

Mineralogy

The studied tuff samples predominantly exhibit freshness, with the amorphous glassy component making up 40.9–94 wt.% of their composition (Fig. 2; Table 2). The presence of volcanic glass and possibly amorphous silica (i.e. opal-A) is suggested by the prominent 15–35°2θ hump in most of the XRD traces. Notably, exceptions are observed in the Poljanska and Ostrožac samples, where the glass content is relatively small or absent, respectively. Ostrožac is characterized by a dominance of secondary calcite (84.3 wt.%), while Poljanska prominently features analcime (41 wt.%). Tuff samples rich in glass content are further characterized with the presence of illite-smectite (1.5–52.3 wt.%), along with minor quantities of quartz (0.5–7.8 wt.%) and plagioclase (3–16.9 wt.%). Illite-smectite, when identified, displays a prominent 001 reflection at approximately 13.5–12.5 Å. The periodicity of illite-smectite is small, and the sole remaining reflex is observed at around 4.55 Å, potentially corresponding to the asymmetric 02*l* (020) diffraction system of phyllosilicates as described by Brindley and Brown (1980). The overall glass/clay ratio in the analyzed tuff categorizes most of it as either fresh vitroclastic or altered vitroclastic tuff (Table 1). Detailed optical and electron-beam petrographic studies of

https://doi.org/10.1017/cmn.2024.21 Published online by Cambridge University Press

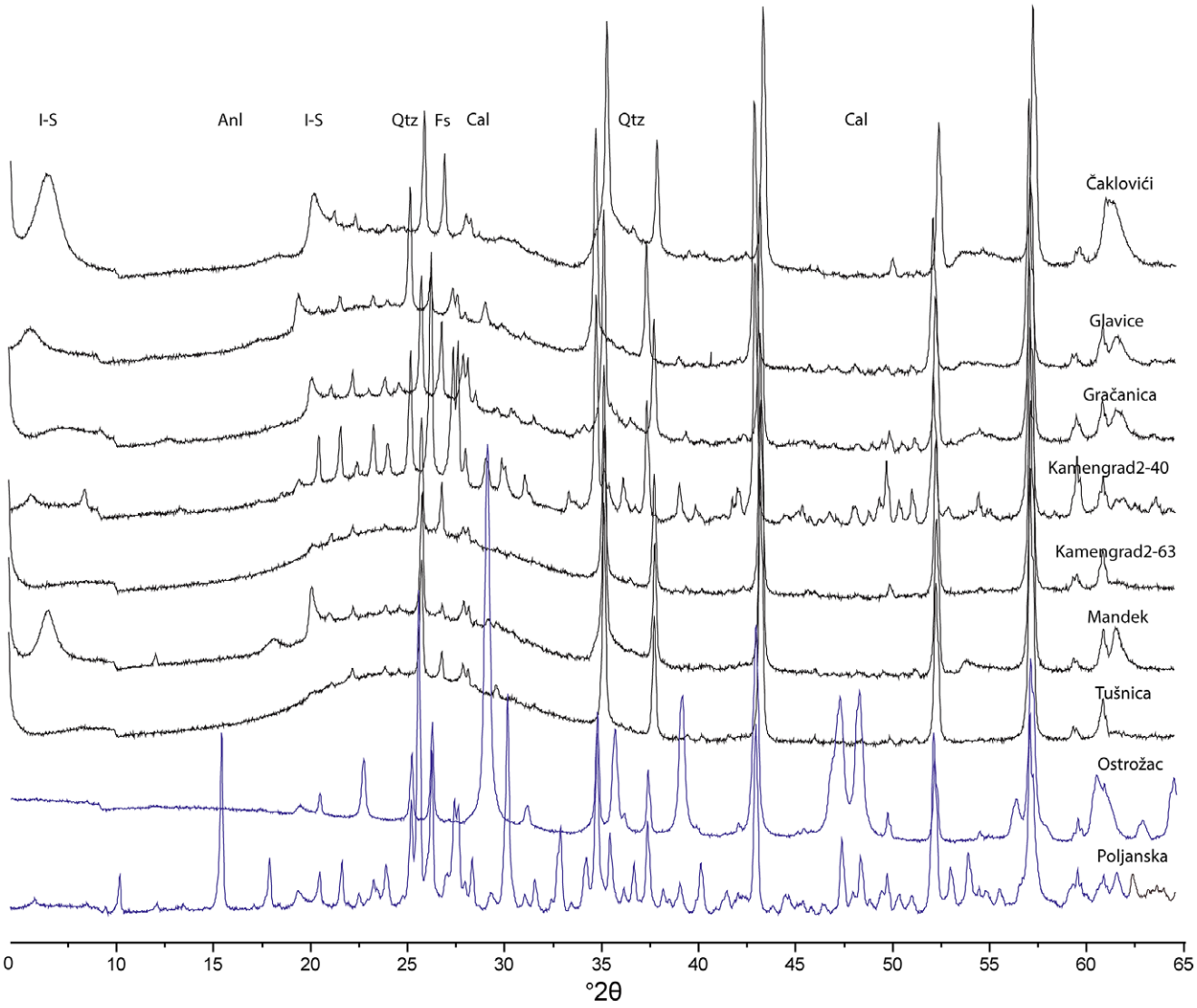

Figure 2. XRD traces of the global fraction of analyzed tuffs. Mineral abbreviations: I-S = illite-smectite; Anl = analcime; Qtz = quartz; Fs = feldspars; Cal = calcite.

Table 2. Rietveld refinement-based mineral quantification (wt.%) of studied tuff

Sample	Illite-smectite	Quartz	Plagioclase	K-feldspar	Analcime	Amorphous matter	Calcite
Gračanica	19.8	2.1	6.8			71.3	
Kamengrad 2.4	8.8	7.8	16.9			66.5	
Kamengrad 2.63	3.4	1.5	3.0			92.1	
Čaklovići	52.3	2.6	4.3			40.9	
Glavice	13.8	1.3	5.0			79.9	
Poljanska	14.8	6.8	16.3	4.9	41.0	16.2	
Tušnica	1.5	0.5	4.0			94.0	
Mandek	18.7	0.8	3.9			76.7	
Ostrožac	5.7	7.5				2.5	84.3

investigated tuff are available in the works of Badurina et al. (2021) and Badurina and Šegvić (2022).

Modelling parameters of mixed-layer minerals consisted of: (1) the orientations of particles on the mounted slides (σ*), (2) the coherent scattering domain sizes expressed in number of layers (CSDS), and (3) the amounts of smectite, kaolinite, and illite in interstratified phases (see Table S2 in the Supplementary material). Considering the paragenesis and crystallinity of I-S, the

https://doi.org/10.1017/cmn.2024.21 Published online by Cambridge University Press

mineralogy of the clay fraction can be categorized into four groups. Group 1 (Mandek and Glavice) is characterized by high crystallinity disordered and ordered illite-smectite (R0 I-SSS, R1 I-SSS; see Table S2 in the Supplementary material). The illite content in R0 I-SSS does not exceed 8%. This aligns with the relative positions of the I-S 002/003 reflexes, along with the 001/002 and 002/003 Δ°2θ values in ethylene glycol-treated traces (see Fig. S1 in the Supplementary material), indicating a smectite-rich (i.e. >90%) illite-smectite (Moore and Reynolds, 1997). Group 2 (Ostrožac and Gračanica) is predominantly composed of multiple generations of well-crystallized and disordered I-S (R0 I-SS), featuring an average of about 20% of an illite component. Detrital illite is also present in this group, while kaolinite-smectite intermediates were observed solely in the Ostrožac sample (see Fig. S1 in the Supplementary material). The samples from Kamengrad2–4, Čaklovići, and Poljanska constitute Group 3. These samples consist of multiple generations of relatively poorly crystalline and disordered illite-smectite (R0 I-SS and R0 I-SSS) with an average illite content of 20%. Discrete illite is likely to be present in these samples. Finally, including samples from Tušnica and Kamengrad2–63, Group 4 exhibits the presence of a variety of I-S with very low crystallinity (see Fig. S1 in the Supplementary material). Modeling these species proved challenging, but it appears that their illite content is significantly greater (about 60%). It is important to note that the samples in this group are rich in amorphous matter (about 90%), while at the same time having the lowest documented abundances of I-S (around 2%; Table 2). Finally, the prominent I-S first basal reflexes documented in all ethylene glycol-solvated traces of analyzed samples, except Čaklovići, revolve around 5.2°2θ (see Fig. S1 in the Supplementary material), which corroborates the random, smectite-rich nature of the present I-S intermediates (Środoń, 1980).

N_2 adsorption–desorption isotherm characteristics

The gas adsorption method serves as a routine approach to determine the specific surface area of fine-grained materials. Analyzing the adsorption isotherm of a non-polar gas such as nitrogen allows for the calculation of the surface area on which a monolayer of adsorbed gas molecules ideally accumulates (Brunauer et al., 1938). Furthermore, the volume of adsorbed gas within meso- and micropores can be assessed by examining hysteresis in the adsorption and desorption isotherms, as well as analyzing the adsorption isotherm at a low partial pressure (Aylmore and Quirk, 1967; Aringhieri, 2004; Michot and Villiéras, 2006; Kaufhold et al., 2010). By analyzing the configuration of the adsorption isotherms and the characteristics of hysteresis loops (Fig. 3), valuable insights

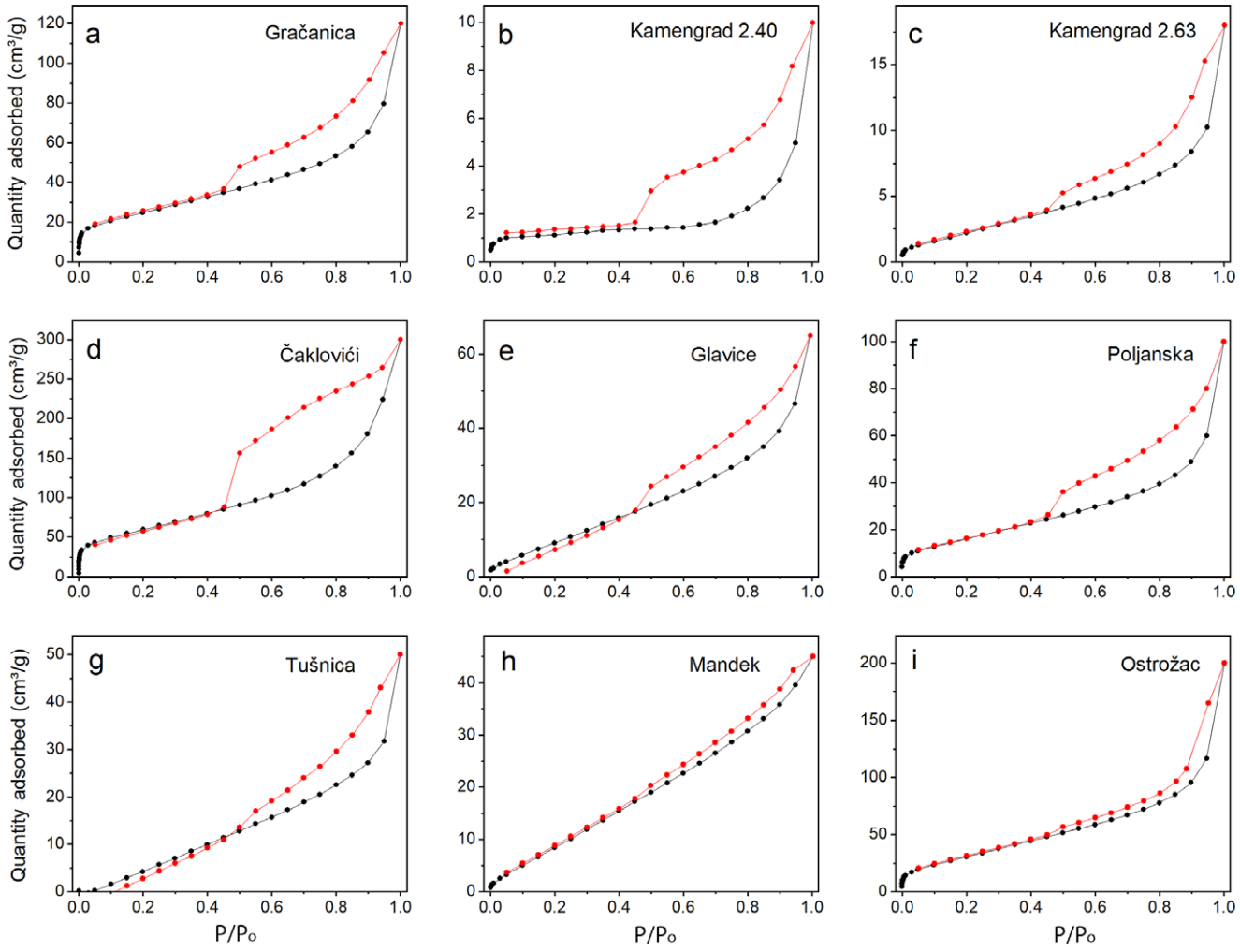

Figure 3. N_2 adsorption–desorption isotherms of studied tuffs. The horizontal axis is the relative pressure (P/P_0), which is the equilibrium pressure divided by the saturation pressure.

https://doi.org/10.1017/cmn.2024.21 Published online by Cambridge University Press

can be derived concerning the adsorption mechanism within analyzed clay minerals, including qualitative indications of the types and geometries of the pores. Considering that the type of exchangeable cation in the interlayer of 2:1 clay minerals can significantly impact the specific surface area (SSA_{N2BET}) and pore volumes of dried powdered samples (Cases et al., 1997; Rutherford et al., 1997), it is worth noting that the clay samples studied had a relatively consistent earth and alkaline earth content (Badurina et al., 2021; Badurina and Šegvić, 2022).

The SEM-EDS investigation revealed that the majority of examined tuffs exhibited a highly compact, laminar arrangement of illite-smectite crystallites. However, in the Čaklovići sample, the illite-smectite morphology seemed rather hairy with an arrangement that resembled a honeycomb or house of cards structure (Badurina and Šegvić, 2022). This is reflected by the differences in shapes of the N_2 adsorption–desorption hysteresis curves between the said sample on one hand and most of the others on the other hand (Fig. 3). These differences become evident at relative pressures exceeding 0.5, which does not directly have an impact on the typical BET range. Additionally, the N_2 adsorption data show notable variations in porosity and SSA_{N2BET} values between the Čaklovići sample and the rest of the dataset. The rest of the dataset shows relative variations in SSA_{N2BET} values which is, given their comparable shape arrangements, probably related to the particle size and the fact that fewer stacked 2:1 layers have more reactive surfaces accessible to the N_2 molecules (Suárez et al., 2022). The average pore size ranged from 19 to 38 Å, with the volume of mesoporosity (20–500 Å) spanning from 0.01 to 0.41 $cm^3\ g^{-1}$, while the contribution of microporosity (<20 Å) was negligible (Table 3).

Rare-earth elements geochemistry

The concentrations of REE (Table 4) were normalized to chondrite (Boynton, 1984) for both glass shards and the clay mineral matrix (Fig. 4). The REE curves exhibit parallel trends, spanning approximately 4–130 times the chondrite content, with total REE content ranging from 65.3 to 394.4 ppm. The geochemical characteristics of volcanic glass highlight its evolved igneous nature, marked by light rare-earth element (LREE) enrichment (La_N/Yb_N = 4.5–6.5) and an Eu anomaly (Eu* = 0.3–0.5). This pattern is also documented in the clay matrix, although certain clay samples show greater LREE/HREE ratios and slightly reduced Eu anomalies. Such trends align with the findings of Badurina et al. (2021), suggesting that the studied tuffs originate from an evolved, intermediate to felsic, magmatic source based on whole-rock tuff geochemistry.

Apart from the Čaklovići and Glavice samples, all mobility curves indicate element loss during the argillitization of volcanic glass (Fig. 5). Moreover, the plots exhibit a range of LREE/HREE ratios, from comparable values (Ostrožac, Kamengrad 2.63) to significant LREE enrichment (Čaklovići, Glavice). Clay fractions extracted from Kamengrad, Glavice, Tušnica, and Ostrožac tuffs exhibit noticeable enrichment in Eu. These positive Eu anomalies are likely to be linked to the prevailing reducing paleoenvironment, causing the preferential mobilization of divalent Eu (Bau, 1991; Yang et al., 2019).

Discussion

Depositional environment conditions and element mobility

Volcanic glass shows inherent instability under low-temperature diagenetic conditions. Upon interaction with water, it easily undergoes transformations into various hydrous phases, such as illite-smectite, which are thermodynamically more stable than glass (Cuadros et al., 1999; Badurina et al., 2021; Gong et al., 2021). The composition of secondary paragenesis is controlled by both the glass composition and environmental physiochemical conditions (Yamamoto et al., 1986; Caballero et al., 1992; dos Muchangos, 2006; Namayandeh et al., 2020). The mechanisms driving the glass alteration include ion diffusion and rearrangement on one hand, and dissolution and precipitation on the other (de la Fuente et al., 2000). In lacustrine, low-temperature (15–25°C; Tütken et al., 2006) and circum-neutral to alkaline regimes (pH 7–8.5; Kříbek et al., 2017), REE are mostly complexed; however, in such solutions LREE appear to be less complexed than HREE. The first form complexes

Table 3. Textural properties obtained from N_2-physisoption isotherms

Sample	SSA ($m^2\ g^{-1}$)	SSA (*t*-plot) ($m^2\ g^{-1}$)	Micropore volume ($cm^3\ g^{-1}$)	Mesopore volume ($cm^3\ g^{-1}$)	Average pore diameter (Å)
Gračanica *Gacko Basin*	89	96	Negligible	0.15	38
Kamengrad2.4	4	2.3 external 1.6 micropore	0.8×10^{-3}	0.01	19
Kamengrad2.63	8	15	Negligible	0.02	35
Čaklovići *Tuzla Basin*	214	241	Negligible	0.41	34
Glavice *Sinj Basin*	39	80	Negligible	0.07	32
Poljanska p. *NCB*	59	79	Negligible	0.12	32
Ostrožac *LTB*	115	168	Negligible	0.24	36
Mandek	39	83	Negligible	0.06	33
Tušnica *Livno Basin*	16	67	Negligible	0.05	32

NCB = North Croatian Basin; LTB = Livno-Tomislavgrad Basins.

https://doi.org/10.1017/cmn.2024.21 Published online by Cambridge University Press

Table 4. LA-ICP-MS geochemistry of rare-earth elements in both shards and the clay matrix of the studied tuffs

Sample	Basin	Material	La	Ce	Pr	Nd	Sm	Eu	Gd	Tb	Dy	Ho	Er	Tm	Yb	Lu	∑REE
Gračanica	Gacko	Clay	14.5	30.2	3.0	10.3	1.9	0.3	1.5	0.2	1.3	0.3	0.8	0.1	0.8	0.1	65.3
		Shards	26.3	51.3	5.1	17.3	3.3	0.5	2.8	0.5	3.0	0.6	1.9	0.3	2.0	0.3	115.2
Kamen.2.40	Kamengrad	Clay	19.5	91.6	4.4	14.9	2.9	0.5	2.6	0.4	2.4	0.5	1.4	0.2	1.6	0.2	143.1
		Shards	23.3	42.9	4.2	14.0	2.7	0.4	2.8	0.4	3.0	0.6	1.9	0.3	2.4	0.4	99.3
Kamen.2.63	Kamengrad	Clay	40.3	96.6	7.6	25.1	4.5	0.7	4.0	0.6	4.1	0.8	2.3	0.4	3.1	0.5	190.6
		Shards	35.1	66.2	6.4	20.7	3.9	0.5	3.2	0.5	3.6	0.8	2.4	0.4	2.6	0.4	146.7
Čaklovići	Tuzla	Clay	87.3	163.5	19.7	72.9	13.8	1.5	12.3	1.8	10.3	1.8	4.5	0.6	3.9	0.5	394.4
		Shards	35.1	72.6	7.4	26.2	5.0	0.6	4.6	0.8	4.8	1.0	2.9	0.4	3.0	0.4	164.8
Glavice	Sinj	Clay	78.3	144.8	15.5	50.9	7.6	1.0	6.2	0.9	5.1	0.9	2.5	0.3	2.3	0.3	316.6
		Shards	35.1	66.6	6.3	21.0	3.8	0.4	3.2	0.5	3.3	0.7	2.2	0.4	2.5	0.4	146.4
Poljanska	NCB	Clay	19.5	48.6	5.3	20.1	4.5	0.3	4.3	0.7	4.0	0.7	1.8	0.3	1.7	0.2	112
		Shards	23.7	56.6	6.4	24.6	6.0	0.4	5.9	1.0	6.7	1.4	4.4	0.6	4.5	0.7	142.9
Tušnica*	Livno	Clay	27.7	57.2	6.5	24.3	4.9	0.6	4.0	0.6	3.5		1.8		1.5	0.2	132.8
		Shards	17.8	40.4	4.9	20.0	5.2	0.5	5.5	0.9	6.0		3.6		3.5	0.5	108.8
Mandek**	Livno	Clay	25.0	154.9	6.0	22.0	4.7	0.7	4.8	0.8	5.0	1.0	2.9	0.5	3.6	0.5	232.4
Ostrožac**	LTB	Clay	17.1	32.7	3.5	12.2	2.1	0.5	1.9	0.3	1.9	0.4	1.3	0.2	1.6	0.2	75.9

Concentrations are expressed in ppm. *Data from Badurina and Šegvić (2022); **glass shards not present. NCB = North Croatian Basin; LTB = Livno-Tomislavgrad Basin.

with Cl^{-}, SO_4^{2-}, and CO_3^{2-}, while the second are commonly associated with CO_3^{2-} (Valsami and Cann, 1992; Li et al., 2019; Gong et al., 2021; Šegvić et al., 2023b). This means that illite-smectite, a phase newly formed through the volcanic glass alteration of studied tuff (Table 2), will have to contend for REE in diagenetic environments with various dissolved anionic species (Cuadros et al., 2023).

The chondrite-normalized REE curves of the clay separates exhibit similar shapes to those of the glass, albeit notable differences exist in terms of total concentrations (Fig. 4). This calls for a relatively large range of fluid/rock ratio environments, which are pivotal in generating fluctuations, both in the enrichment and depletion of REE within the clay fractions (Fig. 5). In instances of REE enrichment the clay mineral hosted adsorption sites clearly prevailed over those associated with dissolved anions. Conversely, REE depletion suggests a deficiency in solid phase binding sites. The larger amount of LREE relative to HREE observed in the studied glass and their clay derivatives is likely to be an artifact of the source magmatism. This interpretation considers the geochemistry of genetically linked Early to Mid-Miocene extension-related felsic and intermediate effusives of the Pannonian Basin (Harangi and Lenkey, 2007; Seghedi and Downes, 2011; Lukács et al., 2018) and their pyroclastic manifestations in the North Croatian Basin and the Dinarides (Šegvić et al., 2014; Badurina et al., 2021; Brlek et al., 2023; Grizelj et al., 2023; Šegvić et al., 2023a; Trinajstić et al., 2023) which all adumbrate LREE/HREE enrichment and negative Eu anomaly. Taking into account the minor variations in the ΣLREE/ΣHREE ratios between fresh glass and their clay alteration products (Fig. 4), relatively equal net losses/gains are inferred, except for the Čaklovići and Glavice samples, which exhibit a notable LREE/HREE enrichment and an overall REE gain in the clay separates (Fig. 5). This cannot be explained by the source geochemistry and is more likely indicative of a preferential dissolution of HREE through carbonate complexation (dos Muchangos, 2006; Badurina and Šegvić, 2022). Limited sorption of such complexes by clay mineral species further aids their depletion in the clay fraction (Byrne and Kim, 1990; Sholkovitz et al., 1994). Given the close proximity of the analyzed tuff beds and lacustrine marls, limestone and/or dolostone (Sunarić et al., 1976; Mandic et al., 2011; Vranjković, 2011; Ćorić et al., 2018; Pavelić et al., 2022), it is reasonable to hypothesize that the paleolake waters in which the studied ash landed were carbonate saturated. This aligns with the conditions observed in many modern karstic lakes (Cantrell and Byrne, 1987; Christidis, 1998). Finally, a detailed inspection of REE mobility curves (Fig. 5) shows that the mobility, and therefore a net loss, of HREE increases proportionally with their greater atomic weight during the alteration of volcanic glass. This heightened mobility is, as already discussed, attributed to HREE complexation in the aqueous phase (Summa and Verosub, 1992). In contrast to the Čaklovići and Glavice tuffs, all the remaining ones exhibit a discernible degree of net REE loss in clay separates (Fig. 5), with the Poljanska and Ostrožac tuffs displaying the most pronounced depletion (50–90%). The significant REE loss may be attributed to the mineralogy of the mentioned two samples which are dominated by zeolite and calcite, respectively, with only a minor presence of clay minerals (Table 2). Compared with phyllosilicates, zeolite and calcite do not fractionate rare-earth elements during low-grade diagenetic processes and their abundances, if any, are generally at trace levels (Terakado and Nakajima, 1995; Cherniak, 1998; Tanaka and Kawabe, 2006).

The mineralogy of the studied tuff indicates a dominant presence of various illite-smectite intermediates (Table 2), which largely lean toward a smectite-rich composition (see Table S2 in the Supplementary material). This observation suggests a slightly basic character of the depositional environment, coupled with the removal of alkalis. These environmental conditions are conducive to the destabilization of glass and feldspars, favoring the preferential formation of smectite over zeolite (Christidis and Huff, 2009; Šegvić et al., 2014; Krajišnik et al., 2019; Feng et al., 2023). In contrast, the Poljanska tuff stands out from this pattern due to its alteration in a saline lake environment (Pavelić et al., 2003). In this specific setting, alkalis persist within the system (Hay, 1964; Hay, 1986). The elevated alkalinity in this environment probably contributed to an increased glass solubility (Mariner and Surdam, 1970), leading to the large-scale formation of zeolite (Table 2).

https://doi.org/10.1017/cmn.2024.21 Published online by Cambridge University Press

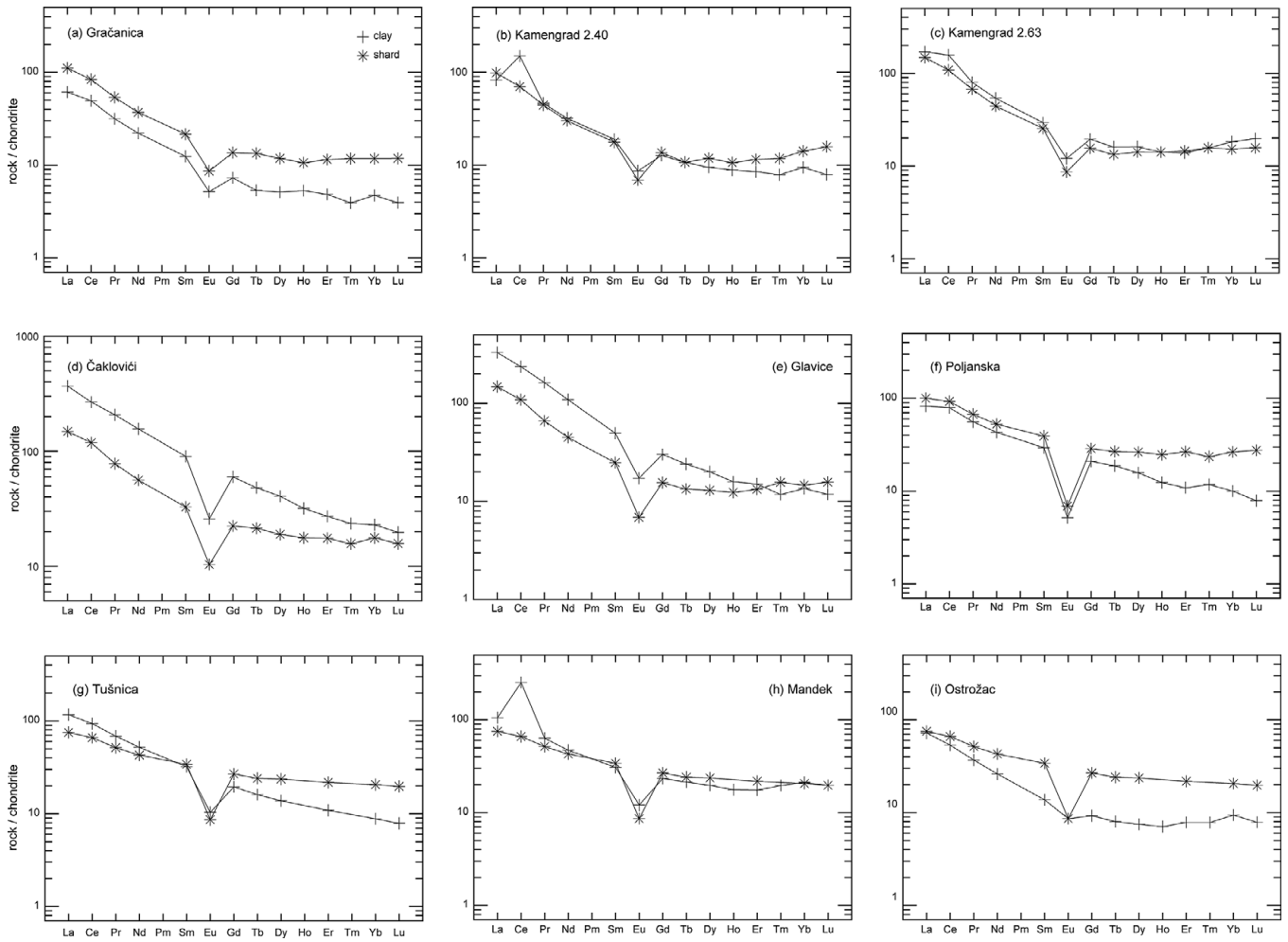

Figure 4. Chondrite-normalized plots of analyzed tuffs.

The prevailing redox conditions during the eogenetic alteration of volcanic glass are readily reflected in the fractionation of redox-sensitive REE, such as Ce and Eu (Elderfield and Greaves, 1982; Bau, 1991; Elderfield et al., 1997; Chen et al., 2015). To illustrate a net change of Ce and Eu that occurred during the argillitization of the studied tuff, their δCe and δEu values were calculated (Liao et al., 2016) (Table 5). When considering δCe, it is noteworthy that all the examined samples exhibit somewhat positive anomalies (ranging from 2.86 to 0.97), apart from the Čaklovići and Glavice samples, which display very weak negative anomalies (ranging from 0.93 to 0.87). This observation is typically associated with redox processes and the partial oxidation of soluble Ce^{3+} to Ce^{4+}. The oxidized form then precipitates *in situ* as CeO_2 (Liu et al., 2022), accumulating in the solid phase, which is dominated by authigenic illite-smectite in the case of the studied altered tuff. The δCe values therefore serve as valuable proxies for assessing the redox environment during the alteration of glass and the subsequent eogenesis of clay minerals (Namayandeh et al., 2020). Following the guidelines proposed by Chen et al. (2015), it becomes evident that these redox conditions varied from oxic (δCe > 1.5, as observed in Kamengrad2.40 and Mandek), to suboxic (δCe ~1.1–1.4, as seen in Kamengrad2.63), and finally to anoxic (δCe < 1.1, observed in the remaining tuff; Table 5). Thicker layers of Kamengrad and Mandek tuffs (2 m and 6 m, respectively) are surmised to have offered a larger volume of porous material for the infiltration of freshwater, thereby fostering a more oxygenated environment during diagenesis. Conversely, thinner and more altered tuff horizons, abundant in less permeable fine-grained carbonate material and authigenic clays, exhibit reduced porosity, leading to limited influx of oxygenated eogenetic fluids (Martizzi et al., 2020).

Regarding the δEu anomaly, the examined tuffs exhibit a broad spectrum of positive δEu values, ranging from 1.03 to 1.69, except for the Čalkovići sample, which registers a value of 0.87 (Table 5). The present authors acknowledge the fact that the Eu anomaly largely stems from inheritance (Fig. 4); this correlation is, however, not universally consistent, and the total intensities of the Eu anomaly were probably influenced by diagenetic conditions. Europium is another highly redox-sensitive lanthanide that, under the prevailing reducing conditions, can undergo transformation into a more soluble divalent form. This transformation ultimately results in the removal of Eu from the solid phase (Bau, 1991; Chen et al., 2015; Yang et al., 2019). The range of δEu values observed in the studied tuff corroborates the assessment of environmental conditions during tuff diagenesis, indicating a predominantly suboxic environment. However, in the case of the Čaklovići tuff, these conditions were notably more reductive. Additional consideration is needed in interpreting δEu values. Unlike Ce, the conversion of Eu^{3+} to Eu^{2+} requires high temperatures (>200°C) (Nagender Nath et al., 1997).

https://doi.org/10.1017/cmn.2024.21 Published online by Cambridge University Press

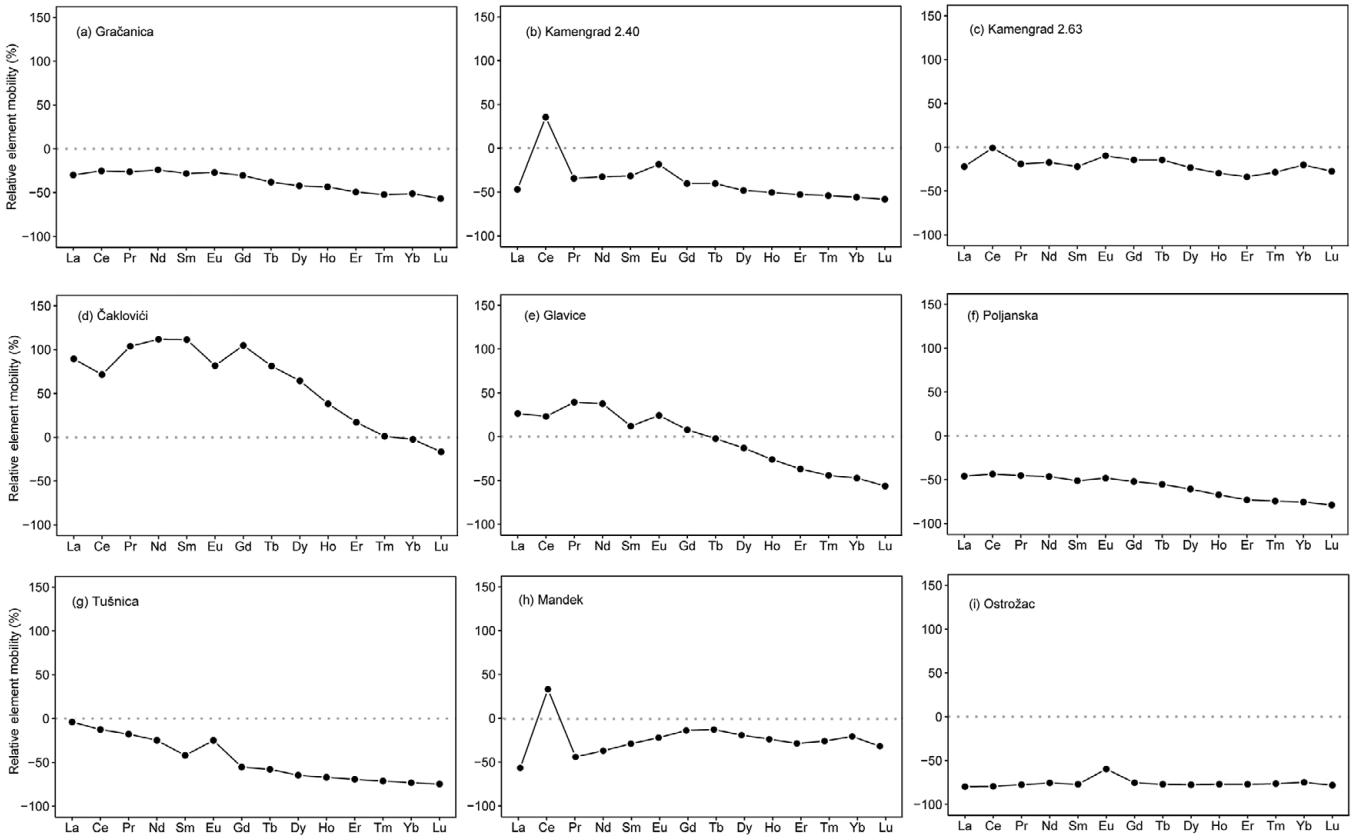

Figure 5. REE mobility plots of analyzed tuffs.

Table 5. Geochemical and mineralogical data synthesis on studied glass shards and clay separates

Sample	ΣREE clay (ppm)	ΣREE glass (ppm)	ΣREE mob	SSA (m^2 g^{-1})	% Amorph.	% I-S	% Sm in I-S	Cryst.	Illite	δCe	δEu	δEu/δCe
Gračanica	65.3	115.2	8.8	96	71.3	19.8	56.4	4	yes	1.04	1.03	0.99
Kamen.2.40	143.1	99.3	8.7	3.9	66.5	8.8	36.5	3	yes	2.30	1.28	0.56
Kamen.2.63	190.6	146.7	11.2	15	92.1	3.4		4		1.25	1.11	0.89
Čaklovići	394.4	164.8	22.6	241	40.9	52.3	69.3	1	no	0.87	0.87	1.00
Glavice	316.6	146.4	13.4	80	79.9	13.8	92	1	no	0.93	1.13	1.22
Poljanska	112	142.9	5.8	79	16.2	14.8		4		1.04	1.07	1.03
Tušnica	132.8*	108.8*	6.8	67	94	1.5	23.5	4	yes	0.98	1.48	1.51
Mandek	232.4		10.6	83	76.7	18.7	82.4	1	no	2.86	1.00	0.35
Ostrožac	75.9		3.4	168	2.5	5.7	40.8	4	yes	0.97	1.69	1.74

Concentrations are expressed in ppm. *Data from Badurina and Šegvić (2022). ΣREE mob = sum of Al normalized ΣREE(clay)/ΣREE(shard) ratios; SSA = specific surface area of clay fractions; % Amorph. = share of amorphous matter (glass); % I-S = share of illite-smectite; % Sm in I-S = sum of Sme components in I-S in all present intermediates; Cryst. = crystallinity group (Table 3); $\delta Ce = Ce_N/(La_N \times Pr_N)^{½}$; $\delta Eu = Eu_N/(Gd_N \times Sm_N)^{½}$ (N denotes clay normalization to glass).

The comparatively greater mass of pyroclastic material in the case of Čaklovići tuff (~3 m thick; Ćorić et al., 2018) probably sustained elevated temperatures for an extended duration, facilitating the reductive dissolution of Eu during tuff diagenesis (Christidis and Huff, 2009). Furthermore, the authors of this study posit that microbial activity might have played a role in the reduction of Eu (Castillo et al., 2022) across all the examined tuffs, given the presence of redox-sensitive microorganisms in certain tuffs (Mandek; Badurina et al., 2020). Finally, the δEu/δCe ratio (Table 5) may offer further insights into the weathering conditions of the studied glass. Consequently, greater values correspond to reduced weathering and a greater content of preserved fresh glass, where Eu is predominantly found in its trivalent form (Drake, 1975). Conversely, smaller δEu/δCe ratios, not associated with an oxic environment (δCe > 2), generally indicate increased weathering intensities due to greater proportions of newly formed clays.

https://doi.org/10.1017/cmn.2024.21 Published online by Cambridge University Press

Clay mineral control on REE mobility

Clay minerals, being the predominant by-products of weathering and hydrothermal alterations, typically retain the majority of the REE budget in sedimentary environments (McLennan, 2001; Carloni et al., 2021; Green et al., 2024). This phenomenon is attributed to the smaller crystallite size and pronounced anisotropy of clay minerals, which eventually leads to the development of two distinct charged surfaces – the basal siloxane surfaces carrying a permanent negative charge and the edge or broken-bond surfaces hosting pH-dependent charge sites (Johnston and Tombácz, 2002; Tournassat et al., 2015). Clay minerals, formed through volcanic glass diagenesis inherit the original magmatic REE signatures (Fig. 4). Additionally, they fractionate REE based on the prevailing physiochemical conditions of the environment, such as redox potential (Eh) and pH, in conjunction with factors like their speciation, morphology, crystallinity, or cation exchange capacity (Yang et al., 2019; Namayandeh et al., 2020; Badurina and Šegvić, 2022; Li and Zhou, 2023). This becomes apparent in the instance of the studied tuff, particularly with the Čaklovići and Glavice samples standing out as the sole examples of REE enrichment in the clay fraction (Fig. 5; Table 5). Despite originating in a slightly alkaline environment, akin to most investigated tuffs, these two samples underwent argillitization in a notably more reducing environment. This probably played a role in the adsorption of REE onto illite-smectite surfaces.

The geochemical nature of studied tuffaceous clays and their spatially related volcanic glass particles is relatively similar (Table 5). It follows that the variations in REE content observed in authigenic clay minerals across different tuffs primarily arise from diagenetic processes. The small particle size of illite-smectite directly corresponds to an increased external surface area of individual crystallites. This is attributed to expansive basal surfaces of I-S and a limited number of stacked T-O-T interlayers (Reid-Soukup and Ulery, 2002). These areas are readily accessible to nitrogen molecules, making N_2 adsorption a convenient method for determining the specific surface area (SSA_{N2BET}) of the studied clays (Table 3). The SSA_{N2BET} and calculated porosity values show significant differences between the Čaklovići tuff on one end and the rest of the dataset on the other. Upon comparing them with the cumulative mobile REE (ΣREE_{mob} = Al-normalized (ΣREE_{clay}/ΣREE_{shard}); Nesbitt, 1979) it becomes evident that the Čaklovići tuff stands out prominently. In contrast, the remaining tuffs exhibit a less defined correlation between SSA_{N2BET} and ΣREE_{mob} (Fig. 6a). It follows that the pronounced capacity of the Čaklovići tuff to fractionate REE during diagenetic alteration of tuff is a function of its high SSA_{N2BET} and porosity values (Table 5). The increase in SSA_{N2BET} of smectite layers is probably associated with intraparticle porosity, stemming from the quasi-crystalline overlap region and accessible zones within the interlayer structure (Suárez et al., 2022). Indeed, the particle morphology of the Čaklovići illite-smectite is rather fibrous or hairy compared with illite-smectite from the rest of studied tuff depicting a typical platelet or cornflake texture (Badurina et al., 2021; Badurina and Šegvić, 2022). This wispy or hairy illite-smectite typically has a thickness of only a few hundred angstroms, but its length exhibits considerable variation, extending up to tens of micrometers (Huggett, 2005). This leads to the development of slit-shaped non-basal surfaces or porosity at the edges of particles, thereby influencing the overall SSA_{N2BET} of illite-smectite (Kaufhold et al., 2010). In analyzing the distinctive features of the Čaklovići tuff, a salient consideration pertains to its substantive MgO content, measuring 4.94 wt.%, a marked departure from the composition of other tuffs (Badurina et al., 2021). Given the mineralogy of studied tuffs (Table 2), it may be hypothesized that Mg is largely hosted in illite-smectite, as felsic glass is virtually devoid of it (Christidis and Huff, 2009). Upon integration of Mg into the structural framework of illite-smectite, it will substitute Al in the octahedral sheet, which in turns leads to charge deficit delocalized over the siloxane planes (Sposito et al., 1999). This creates a conducive adsorption environment for solvated cations like LREE, which propagate away from the glass in the guise of 8- or 9-fold hydrated outer-sphere complexes (Borst et al., 2020). Indeed, the large MgO content of Čaklovići clays might have contributed to their LREE retention potential (Fig. 5; Table 5).

To investigate further into the characteristics of I-S that potentially govern the adsorption of REE during tuff alteration, the smectite content of I-S (Table S2; Table 5) was plotted against ΣREE_{mob}. This revealed a strong correlation between these two parameters (Fig. 6b). It appears that REE exhibit a pronounced affinity for the less charged smectite component within the I-S structure. This suggests a potential interaction between the smectite component and REE through surface complexation and/or ion exchange mechanisms. Additionally, the correlation

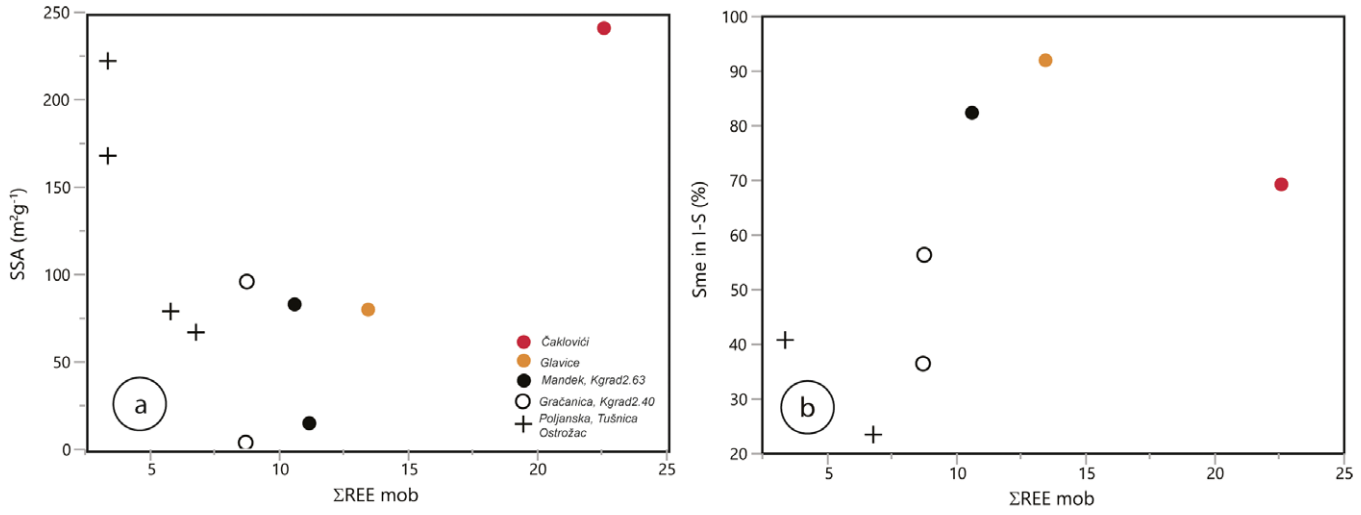

Figure 6. (a) SSA *vs* ΣREE_{mob} and (b) Sme in I-S *vs* ΣREE_{mob} correlation diagrams.

https://doi.org/10.1017/cmn.2024.21 Published online by Cambridge University Press

between the particle size of mixed-layered clay minerals and their surface area exhibits an inverse proportionality (Nadeau et al., 1984). The augmentation of smectite layer content within the smallest I-S crystallites therefore implies a concurrent increase in the REE-accessible adsorption surface area (Jaynes and Bigham, 1986; Sposito et al., 1999). Beyond basal surfaces, the presence of variable pH-dependent sites along broken hydroxyl edges of I-S offers additional sites for the complexation of REE (Coppin et al., 2002; Wu et al., 2023). In solutions with a greater alkaline pH, these edges are more favorable to REE adsorption (Awual et al., 2013). Their significance is particularly notable in the context of the Čaklovići tuff, where there is evidence of increased slit-shaped intraparticle porosity along the edges, as suggested by SSA_{N2BET} (Table 5) and corroborated by SEM-EDS data (Badurina et al., 2021). In connection with the noted phenomenon of REE fractionation being most pronounced in smectite-rich I-S, it is noteworthy that the clay fraction of those samples is devoid of discrete illite (Table S2; Table 5). Furthermore, there is no discernible correlation between the overall content of I-S or volcanic glass on one end and the total content of REE associated with authigenic illite-smectite on the other (Table 5). This underscores the leading role of the smectite component of I-S, and to some extent, the particle specific surface area and charge distribution, as primary determinants influencing REE fractionation during volcanic ash diagenesis.

From a regional perspective, it can be inferred that illite-smectite of the altered Miocene tuff of the Southwestern Pannonian Basin and the adjacent Dinarides intramontane basins show a notable capacity as reasonably effective REE scavenging lithologies. Typically, it retains no less than 50% of the REE budget originating from the volcanic source (Fig. 5). Over the course of the Early and Middle Miocene epochs, the areas along the southern perimeter of the Pannonian Basin experienced substantial climatic, tectonic, and eustatic transformations. These engendered a range of depositional environments, encompassing lacustrine to marine settings, with coal beds frequently defining the deposition environment for the tuffs (Pavelić et al., 2003; Pavelić and Kovačić 2018; Mandic et al., 2019a; Mandic et al., b; Pavelić et al., 2022). The prevailing suboxic to reducing conditions, and a relatively alkaline nature, proved favorable to the adsorption of REE on illite-smectite. This phenomenon was particularly pronounced in transitional lacustrine to marine settings, as exemplified by the Čaklovići tuff (Fig. 1), where highly reactive, smectite-rich I-S developed from the glassy substrate.

Conclusions

This study investigated the complex interplay between depositional environment conditions, volcanic glass alteration, and the subsequent authigenesis of clay minerals in Miocene SPB and DIB tuffs on one hand and then the ability of clay minerals to fractionate REE on the other hand. The normalized REE patterns of clay mineral separates demonstrate similarities to those of the glass, albeit with variations in total concentrations. These variations suggest a significant range of fluid/rock ratios, crucial in determining fluctuations in REE enrichment and depletion within the clay fractions. The source magmatism geochemistry contributes to the observed patterns of REE distribution. Notably, the distinct LREE/HREE enrichment and negative Eu anomaly align with the characteristics of Early to Mid-Miocene extension-related magmatism in the Pannonian Basin.

The redox conditions during the eogenetic alteration of volcanic glass are reflected in the fractionation of redox-sensitive REE such as Ce and Eu. The calculated δCe and δEu values provide valuable insights into the redox environment during tuff diagenesis, indicating variations from oxic to anoxic conditions across different samples. The subtle positive correlation between δEu and δCe hints at a potential influence of coal-bearing layers within the same diagenetic environment. This study demonstrated that illite-smectite, formed through volcanic glass diagenesis, inherits magmatic REE signatures and fractionates REE based on prevailing physiochemical conditions. The particle properties of illite-smectite, including specific surface area and porosity, also influence its REE fractionation capacity, with the Čaklovići tuff standing out prominently due to its unique characteristics. Moreover, a correlation between smectite content in illite-smectite and a total amount of fractionated REE draws attention to the significant role of smectite layers in REE fractionation during volcanic ash diagenesis. In conclusion, the altered Miocene tuffs in the SPB and DIB serve as a noteworthy REE scavenger, retaining a substantial portion of the REE budget from the volcanic glass. Additional research is needed, however, to assess the economic potential of such ion adsorption clays.

Supplementary material. The supplementary material for this article can be found at http://doi.org/10.1017/cmn.2024.21.

Author contributions. **Branimir Šegvić:** Conceptualization, Methodology, Validation, Formal Analysis, Investigation, Resources, Data Curation, Supervision, Writing – Original Draft, Visualization, Funding Acquisition; **Luka Badurina:** Conceptualization, Methodology, Investigation, Data Curation, Resources, Writing – Review & Editing, Funding Acquisition; **Adriano E. Braga:** Formal Analysis, Investigation, Resources, Writing – Review & Editing; **Oleg Mandic:** Investigation, Writing – review & editing; **Damir Slovenec:** Writing – review & editing; **Kevin Werts:** Resources, Writing – review & editing; **Emily Doyle:** Formal Analysis; **Frane Marković:** Resources; **Goran Slivišek:** Resources; **Vedad Demir:** Resources.

Acknowledgements. The authors thank Svetlana Renovica ('Rudnik i termoelektrana Ugljevik'), Boško Vuković ('Rudnik Gacko') and Tvrtko Ćubela (Livno) as well as Sejfudin Vrabac and Elvir Babajić from the University of Tuzla and Hazim Hrvatović from the Federal Geological Survey Sarajevo for their great help during the field work. Kevin Byerly is thanked for the constructive comments he provided during the preparation of this manuscript. We greatly appreciate the assistance of Ebunoluwa Olowolayemo for his fantastic support with the English, ensuring improved clarity, style, and grammar throughout this work. Finally, the critical comments and constructive reviews by Paul A. Schroeder and one anonymous reviewer, as well as editorial handling by Joseph W. Stucki have contributed significantly to the quality of this paper.

Financial support. The research received support from the Portnoy Geology Solidus Fund and the Texas Tech Geoscience Society, as well as the Geosciences Clay Laboratory of Texas Tech University.

Competing interests. The authors declare that they have no known competing financial interests or personal relationships that could have appeared to influence the work reported in this paper.

Data availability statement. Additional data supporting the findings of this study are available from the corresponding author, Branimir Šegvić, upon request.

References

Alonso, E., Sherman, A.M., Wallington, T.J., Everson, M.P., Field, F.R., Roth, R., & Kirchain, R.E. (2012). Evaluating rare earth element availability: a case with

revolutionary demand from clean technologies. *Environmental Science & Technology*, *46*, 3406–3414.

Andrić, N., Sant, K., Matenco, L., Mandic, O., Tomljenović, B., Pavelić, D., Hrvatović, H., Demir, V., & Ooms, J. (2017). The link between tectonics and sedimentation in asymmetric extensional basins: inferences from the study of the Sarajevo-Zenica Basin. *Marine and Petroleum Geology*, *83*, 305–332.

Andrić-Tomašević, N., Simić, V., Mandic, O., Životić, D., Suárez, M., & García-Romero, E. (2021). An arid phase in the Internal Dinarides during the early to middle Miocene: Inferences from Mg-clays in the Pranjani Basin (Serbia). *Palaeogeography, Palaeoclimatology, Palaeoecology*, *562*, 110145.

Aringhieri, R. (2004). Nanoporosity characteristics of some natural clay minerals and soils. *Clays and Clay Minerals*, *52*, 700–704.

Awual, M.R., Kobayashi, T., Shiwaku, H., Miyazaki, Y., Motokawa, R., Suzuki, S., Okamoto, Y., & Yaita, T. (2013). Evaluation of lanthanide sorption and their coordination mechanism by EXAFS measurement using novel hybrid adsorbent. *Chemical Engineering Journal*, *225*, 558–566.

Aylmore, L., & Quirk, J. (1967). The micropore size distributions of clay mineral systems. *Journal of Soil Science*, *18*, 1–17.

Bada, G., & Horváth, F. (2001). On the structure and tectonic evolution of the Pannonian Basin and surrounding orogens. *Acta Geologica Hungarica*, *44*, 301–327.

Badurina, L., & Šegvić, B. (2022). Assessing trace-element mobility during alteration of rhyolite tephra from the Dinaride Lake System using glass-phase and clay-separate laser ablation inductively coupled plasma mass spectrometry. *Clay Minerals*, *57*, 1–6.

Badurina, L., Šegvić, B., Mandic, O., & Zanoni, G. (2020). Smectitization as a trigger of bacterially mediated Mn-Fe micronodule generation in felsic glass (Livno-Tomislavgrad Paleolake, *Bosnia and Herzegovina).* Minerals, *10*, 899.

Badurina, L., Šegvić, B., Mandic, O., & Slovenec, D. (2021). Miocene tuffs from the Dinarides and Eastern Alps as proxies of the Pannonian Basin lithosphere dynamics and tropospheric circulation patterns in Central Europe. *Journal of the Geological Society*, *178*, 1–18.

Bakrač, K., Hajek-Tadesse, V., Miknić, M., Grizelj, A., Hećimović, I., & Kovačić, M. (2010). Evidence for Badenian local sea level changes in the proximal area of the North Croatian Basin. *Geologia Croatica*, *63*, 259–269.

Balaram, V. (2019). Rare earth elements: review of applications, occurrence, exploration, analysis, recycling, and environmental impact. *Geoscience Frontiers*, *10*, 1285–1303.

Balla, Z. (1986). Palaeotectonic reconstruction of the central Alpine-Mediterranean belt for the Neogene. *Tectonophysics*, *127*, 213–243.

Barrett, E.P., Joyner, L.G., & Halenda, P.P. (1951). The determination of pore volume and area distributions in porous substances. I. Computations from nitrogen isotherms. *Journal of the American Chemical Society*, *73*, 373–380.

Bau, M. (1991). Rare-earth element mobility during hydrothermal and metamorphic fluid-rock interaction and the significance of the oxidation state of europium. *Chemical Geology*, *93*, 219–230.

Berti, D., Slowey, N.C., Yancey, T.E., & Deng, Y. (2022). Rare earth nanominerals in bentonite deposits of the Eocene Texas coastal plains. *Applied Clay Science*, *216*, 106373.

Berti, D., Slowey, N.C., Deng, Y., Yancey, T.E., & Velazquez, A.L.B. (2023). Yttrium and REE mineralization in manganese pods occurring in bentonite deposits of the Eocene Texas Coastal Plain. *Clays and Clay Minerals.*, *71*, 253–273.

Binnemans, K., Jones, P.T., Blanpain, B., Van Gerven, T., Yang, Y., Walton, A., & Buchert, M. (2013). Recycling of rare earths: a critical review. *Journal of Cleaner Production*, *51*, 1–22.

Borst, A.M., Smith, M.P., Finch, A.A., Estrade, G., Villanova-de-Benavent, C., Nason, P., Marquis, E., Horsburgh, N.J., Goodenough, K.M., Xu, C., Kynický, J., & Geraki, K. (2020). Adsorption of rare earth elements in regolith-hosted clay deposits. *Nature Communications*, *11*, 4386.

Boynton, W.V. (1984). Chapter 3 – Cosmochemistry of the rare earth elements. In *Developments in Geochemistry* (ed. P. Henderson), *2*, 63–114. Elsevier.

Brigatti, M.F., Galán, E., & Theng, B.K.G. (2013). Chapter 2 – Structure and mineralogy of clay minerals. In *Developments in Clay Science* (ed. F. Bergaya and G. Lagaly), pp. 21–81). Elsevier.

Brindley, G.W., & Brown, G. (eds) (1980). *Crystal Structures of Clay Minerals and their X-Ray Identification*. Mineralogical Society of Great Britain and Ireland.

Brlek, M., Richard Tapster, S., Schindlbeck-Belo, J., Gaynor, S.P., Kutterolf, S., Hauff, F., Georgiev, S.V., Trinajstić, N., Šuica, S., Brčić, V., Wang, K.-L., Lee, H.-Y., Beier, C., Abersteiner, A.B., Mišur, I., Peytcheva, I., Kukoč, D., Németh, B., Trajanova, M., Balen, D., Guillong, M., Szymanowski, D., & Lukács, R. (2023). Tracing widespread Early Miocene ignimbrite eruptions and petrogenesis at the onset of the Carpathian-Pannonian Region silicic volcanism. *Gondwana Research*, *116*, 40–60.

Brugger, J., Ogierman, J., Pring, A., Waldron, H., & Kolitsch, U. (2006). Origin of the secondary REE-minerals at the Paratoo copper deposit near Yunta, South Australia. *Mineralogical Magazine*, *70*, 609–627.

Brunauer, S., Emmett, P.H., & Teller, E. (1938). Adsorption of gases in multimolecular layers. *Journal of the American Chemical Society*, *60*, 309–319.

Burkov, V.V., & Podporina, Y.K. (1967). Rare-earths in granitoid residuum. U.S.S.R. Doklady Academy of Sciences, Earth Science Section, pp. 214–216.

Byrne, R.H., & Kim, K.-H. (1990). Rare earth element scavenging in seawater. *Geochimica et Cosmochimica Acta*, *54*, 2645–2656.

Caballero, E., Reyes, E., Delgado, A., Huertas, F., & Linares, J. (1992). The formation of bentonite: mass balance effects. *Applied Clay Science*, *6*, 265–276.

Cantrell, K.J., & Byrne, R.H. (1987). Rare earth element complexation by carbonate and oxalate ions. *Geochimica et Cosmochimica Acta*, *51*, 597–605.

Carloni, D., Šegvić, B., Sartori, M., Zanoni, G., Moscariello, A., & Besse, M. (2021). Raw material choices and material characterization of the 3rd and 2nd millennium BC pottery from the Petit-Chasseur necropolis: insights into the megalith-erecting society of the Upper Rhône Valley, Switzerland. *Geoarchaeology*, *36*, 1009–1044.

Cases, J.M., Bérend, I., François, M., Uriot, L.P., Michot, L.J., & Thomas, F. (1997). Mechanism of adsorption and desorption of water vapor by homoionic montmorillonite: 3. The Mg^{2+}, Ca^{2+}, Sr^{2+} and Ba^{2+} exchanged forms. *Clays and Clay Minerals*, *45*, 8–22.

Castillo, J., Maleke, M., Unuofin, J., Cebekhulu, S., & Gómez-Arias, A. (2022). Microbial recovery of rare earth elements. In *Environmental Technologies to Treat Rare Earth Element Pollution: Principles and Engineering* (ed. A. Sinharoy & P.N.L. Lens). IWA Publishing.

Chen, J., Algeo, T.J., Zhao, L., Chen, Z.-Q., Cao, L., Zhang, L., & Li, Y. (2015). Diagenetic uptake of rare earth elements by bioapatite, with an example from Lower Triassic conodonts of South China. *Earth-Science Reviews*, *149*, 181–202.

Cherniak, D.J. (1998). REE diffusion in calcite. *Earth and Planetary Science Letters*, *160*, 273–287.

Cheshire, M.C., Bish, D.L., Cahill, J.F., Kertesz, V., & Stack, A.G. (2018). Geochemical evidence for rare-earth element mobilization during kaolin diagenesis. *ACS Earth and Space Chemistry*, *2*, 506–520.

Christidis, G.E. (1998). Comparative study of the mobility of major and trace elements during alteration of an andesite and a rhyolite to bentonite, in the Islands of Milos and Kimolos, Aegean, Greece. *Clays and Clay Minerals*, *46*, 379–399.

Christidis, G.E., & Huff, W.D. (2009). Geological aspects and genesis of bentonites. *Elements*, *5*, 93–98.

Coppin, F., Berger, G., Bauer, A., Castet, S., & Loubet, M. (2002). Sorption of lanthanides on smectite and kaolinite. *Chemical Geology*, *182*, 57–68.

Ćorić, S., Vrabac, S., Đulović, I., & Babajić, E. (2018). The Lower Miocene and the Lower Badenian on the Čaklovići cross section in Tuzla Basin, pp. 115–120. Conference Proceedings, Vrnjačka Banja.

Cornu, S., Deschatrettes, V., Salvador-Blanes, S., Clozel, B., Hardy, M., Branchut, S., & Le Forestier, L. (2005). Trace element accumulation in Mn-Fe-oxide nodules of a planosolic horizon. *Geoderma*, *125*, 11–24.

Csontos, L., & Vörös, A. (2004). Mesozoic plate tectonic reconstruction of the Carpathian region. *Palaeogeography, Palaeoclimatology, Palaeoecology*, *210*, 1–56.

Csontos, L., Nagymarosy, A., Horváth, F., & Kovác, M. (1992). Tertiary evolution of the Intra-Carpathian area: a model. *Tectonophysics*, *208*, 221–241.

Cuadros, J., Caballero, E., Huertas, F.J., Jiménez de Cisneros, C., Huertas, F., & Linares, J. (1999). Experimental alteration of volcanic tuff: smectite formation and effect on ^{18}O isotope composition. *Clays and Clay Minerals*, *47*, 769–776.

https://doi.org/10.1017/cmn.2024.21 Published online by Cambridge University Press

Cuadros, J., Mavris, C., & Nieto, J.M. (2023). Rare earth element signature modifications induced by differential acid alteration of rocks in the Iberian Pyrite Belt. *Chemical Geology*, *619*, 121323.

Cunningham, M.J., Lowe, D.J., Wyatt, J.B., Moon, V.G., & Churchman, G.J. (2016). Discovery of halloysite books in altered silicic Quaternary tephras, northern New Zealand. *Clay Minerals*, *51*, 351–372.

Dapiaggi, M., Pagliari, L., Pavese, A., Sciascia, L., Merli, M., & Francescon, F. (2015). The formation of silica high temperature polymorphs from quartz: influence of grain size and mineralising agents. *Journal of the European Ceramic Society*, *35*, 4547–4555.

Daumann, L.J., Pol, A., Op den Camp, H.J.M., & Martinez-Gomez, N.C. (2022). Chapter 1 – A perspective on the role of lanthanides in biology: discovery, open questions and possible applications. In *Advances in Microbial Physiology*, pp. 1–24 (ed. R.K. Poole & D.J. Kelly). Academic Press.

de la Fuente, S., Cuadros, J., Fiore, S., & Linares, J. (2000). Electron microscopy study of volcanic tuff alteration to illite-smectite under hydrothermal conditions. *Clays and Clay Minerals*, *48*, 339–350.

de Leeuw, A., Mandic, O., de Bruijn, H., Marković, Z., Reumer, J., Wessels, W., Šišić, E., & Krijgsman, W. (2011). Magnetostratigraphy and small mammals of the Late Oligocene Banovići basin in NE Bosnia and Herzegovina. *Palaeogeography, Palaeoclimatology, Palaeoecology*, *310*, 400–412.

de Leeuw, A., Mandic, O., Krijgsman, W., Kuiper, K., & Hrvatović, H. (2012). Paleomagnetic and geochronologic constraints on the geodynamic evolution of the Central Dinarides. *Tectonophysics*, *530–531*, 286–298.

Dileep Kumar, M. (1984). Ionic potential correlations with chemical processes of rare earths in the sea. *Marine Chemistry*, *14*, 253–258.

Doebelin, N., & Kleeberg, R. (2015). Profex: a graphical user interface for the Rietveld refinement program BGMN. *Journal of Applied Crystallography*, *48*, 1573–1580.

dos Muchangos, A.C. (2006). The mobility of rare-earth and other elements in the process of alteration of rhyolitic rocks to bentonite (Lebombo Volcanic Mountainous Chain, Mozambique). *Journal of Geochemical Exploration*, *88*(1), 300–303. https://doi.org/10.1016/j.gexplo.2005.08.061

Drake, M.J. (1975). The oxidation state of europium as an indicator of oxygen fugacity. *Geochimica et Cosmochimica Acta*, *39*, 55–64.

Drits, V.A., & Sakharov, B.A. (1976). *X-Ray Structural Analysis of Mixed-Layer Minerals*, 256 pp. Nauka, Moscow, Russian Federation.

Dubinin, A.V. (2004). Geochemistry of rare earth elements in the ocean. *Lithology and Mineral Resources*, *39*, 289–307.

Elderfield, H., & Greaves, M.J. (1982). The rare earth elements in seawater. *Nature*, *296*, 214–219.

Elderfield, H., Whitfield, M., Burton, J.D., Bacon, M.P., Liss, P.S., Charnock, H., Lovelock, J.E., Liss, P.S., & Whitfield, M. (1997). The oceanic chemistry of the rare-earth elements. *Philosophical Transactions of the Royal Society of London. Series A, Mathematical and Physical Sciences*, *325*, 105–126.

Elliott, W.C. (2020). Regolith-hosted rare-earth elements: phyllosilicate connection. *American Mineralogist*, *105*, 1–2.

Ercan, H.Ü., Ece, Ö.I., Çiftçi, E., & Aydın, A. (2022). Comparison of epithermal kaolin deposits from the Etili Area (Çanakkale, Turkey): mineralogical, geochemical, and isotopic characteristics. *Clays and Clay Minerals*, *70*, 753–779.

Feng, M., Kou, Z., Tang, C., Shi, Z., Tong, Y., & Zhang, K. (2023). Recent progress in synthesis of zeolite from natural clay. *Applied Clay Science*, *243*, 107087.

Ferrage, E., Lanson, B., Sakharov, B.A., Geoffroy, N., Jacquot, E., & Drits, V.A. (2007). Investigation of dioctahedral smectite hydration properties by modeling of X-ray diffraction profiles: influence of layer charge and charge location. *American Mineralogist*, *92*, 1731–1743.

Gifkins, C.C., & Allen, R.L. (2001). Textural and chemical characteristics of diagenetic and hydrothermal alteration in glassy volcanic rocks: examples from the Mount Read Volcanics, Tasmania. *Economic Geology*, *96*, 973–1002.

Gismondi, P., Kuzmin, A., Unsworth, C., Rangan, S., Khalid, S., & Saha, D. (2022). Understanding the adsorption of rare-earth elements in oligo-grafted mesoporous carbon. *Langmuir*, *38*, 203–210.

Gong, Q., Li, F., Lu, C., Wang, H., & Tang, H. (2021). Tracing seawater- and terrestrial-sourced REE signatures in detritally contaminated, diagenetically altered carbonate rocks. *Chemical Geology*, *570*, 120169.

Green, H., Šegvić, B., Luka, Badurina, L., Omodeo-Salé, S., & Le Bayon, R. (2024). Grain size control on organo-clay complexation and REE fractionation in the Paleozoic strata of the Permian Basin (West Texas, U.S.A.). *Journal of Sedimentary Research*, *94*(4), 488–503. https://doi.org/10.2110/jsr.2024.007

Grizelj, A., Milošević, M., Bakrač, K., Galović, I., Kurečić, T., Hajek-Tadesse, V., Avanić, R., Miknić, M., Horvat, M., Janković, A.Č., & Matošević, M. (2020). Paleoecological and sedimentological characterisation of Middle Miocene sediments from the Hrvatska Kostajnica area (Croatia). *Geologia Croatica*, *73*.

Grizelj, A., Milošević, M., Miknić, M., Hajek-Tadesse, V., Bakrač, K., Galović, I., Badurina, L., Kurečić, T., Wacha, L., Šegvić, B., Matošević, M., Čaić-Janković, A., & Avanić, R. (2023). Evidence of Early Sarmatian volcanism in the Hrvatsko Zagorje Basin, Croatia: mineralogical, geochemical and biostratigraphic approaches. *Geologica Carpathica*, *74*, 59–82.

Gupta, C.K., & Krishnamurthy, N. (1992). Extractive metallurgy of rare earths. *International Materials Reviews*, *37*, 197–248.

Gverić, Z., Hanžel, D., Kampić, Š., Pleša, A., & Tibljaš, D. (2020). Comprehensive characterization of bentonites from Croatia and neighboring countries. *Geologia Croatica*, *73*, 29–48.

Hajek-Tadesse, V., Wacha, L., Horvat, M., Galović, I., Bakrač, K., Grizelj, A., Mandic, O., & Reichenbacher, B. (2023). New evidence for Early Miocene palaeoenvironmental changes in the North Croatian Basin: insights implicated by microfossil assemblages. *Geobios*, *77*, 1–25.

Hao, W., Flynn, S.L., Kashiwabara, T., Alam, M.S., Bandara, S., Swaren, L., Robbins, L.J., Alessi, D.S., & Konhauser, K.O. (2019). The impact of ionic strength on the proton reactivity of clay minerals. *Chemical Geology*, *529*, 119294.

Harangi, S., & Lenkey, L. (2007). Genesis of the Neogene to Quaternary volcanism in the Carpathian-Pannonian region: role of subduction, extension, and mantle plume. *Geological Society of America*, *418*, 67.

Harangi, S., Lukács, R., Schmitt, A.K., Dunkl, I., Molnár, K., Kiss, B., Seghedi, I., Novothny, & Molnár, M. (2015). Constraints on the timing of Quaternary volcanism and duration of magma residence at Ciomadul volcano, east-central Europe, from combined U-Th/He and U-Th zircon geochronology. *Journal of Volcanology and Geothermal Research*, *301*, 66–80.

Hay, R.L. (1964). Phillipsite of saline lakes and soils. *American Mineralogist*, *49*, 1366–1387.

Hay, R.L. (1986). Geologic occurrence of zeolites and some associated minerals. In *Studies in Surface Science and Catalysis* (ed. Y. Murakami, A. Iijima, & J.W. Ward), pp. 35–40. Elsevier.

Holbourn, A., Kuhnt, W., Kochhann, K.G.D., Andersen, N., & Meier, K.J.S. (2015). Global perturbation of the carbon cycle at the onset of the Miocene Climatic Optimum. *Geology*, *43*, 123–126.

Hollocher, K., & Ruiz, J. (1995). Major and trace element determinations on NIST glass standard reference materials 611, 612, 614 and 1834 by inductively coupled plasma-mass spectrometry. *Geostandards Newsletter*, *19*, 27–34.

Hong, H., Fang, Q., Wang, C., Churchman, G.J., Zhao, L., Gong, N., & Yin, K. (2017). Clay mineralogy of altered tephra beds and facies correlation between the Permian-Triassic boundary stratigraphic sets, Guizhou, South China. *Applied Clay Science*, *143*, 10–21.

Horváth, F. (1995). Phases of compression during the evolution of the Pannonian Basin and its bearing on hydrocarbon exploration. *Marine and Petroleum Geology*, *12*, 837–844.

Horváth, F., Bada, G., Szafián, P., Tari, G., Ádám, A., & Cloetingh, S. (2006). Formation and deformation of the Pannonian Basin: constraints from observational data. *Geological Society, London, Memoirs*, *32*, 191–206.

Huff, W.D. (2016). K-bentonites: review. *American Mineralogist*, *101*, 43–70.

Huff, W.D., Bergström, S.M., Kolata, D.R., & Sun, H. (1998). The Lower Silurian Osmundsberg K-bentonite. Part II: Mineralogy, geochemistry, chemostratigraphy and tectonomagmatic significance. *Geological Magazine*, *135*, 15–26.

Huggett, J.M. (2005). Sedimentary Rocks | Clays and Their Diagenesis. In R. C. Selley, L. R. M. Cocks, & I. R. Plimer (Eds.), *Encyclopedia of Geology* (pp. 62–70). Elsevier. https://doi.org/10.1016/B0-12-369396-9/00311-7

Humphries, M. (2010). Rare Earth Elements: The Global Supply Chain. *Congressional Research Service*. 40 pp.

https://doi.org/10.1017/cmn.2024.21 Published online by Cambridge University Press

Jaynes, W.F., & Bigham, J.M. (1986). Multiple cation-exchange capacity measurements on standard clays using a commercial mechanical extractor. *Clays and Clay Minerals*, *34*, 93–98.

Jiménez-Moreno, G., Mandic, O., Harzhauser, M., Pavelić, D., & Vranjković, A. (2008). Vegetation and climate dynamics during the early middle Miocene from Lake Sinj (Dinaride Lake system, *SE Croatia).* Review of Palaeobotany and Palynology, *152*, 237–245.

Jochum, K.P., Willbold, M., Raczek, I., Stoll, B., & Herwig, K. (2005). Chemical characterisation of the USGS reference glasses GSA-1G, GSC-1G, GSD-1G, GSE-1G, BCR-2G, BHVO-2G and BIR-1G using EPMA, ID-TIMS, ID-ICP-MS and LA-ICP-MS. *Geostandards and Geoanalytical Research*, *29*, 285–302.

Johnston, C.T., & Tombácz, E. (2002). Surface chemistry of soil minerals. In *Soil Mineralogy with Environmental Applications*, pp. 37–67. John Wiley & Sons Ltd.

Kaufhold, S., Dohrmann, R., Klinkenberg, M., Siegesmund, S., & Ufer, K. (2010). N2-BET specific surface area of bentonites. *Journal of Colloid and Interface Science*, *349*, 275–282.

Kiipli, T., Hints, R., Kallaste, T., Verš, E., & Voolma, M. (2017). Immobile and mobile elements during the transition of volcanic ash to bentonite – an example from the early Palaeozoic sedimentary section of the Baltic Basin. *Sedimentary Geology*, *347*, 148–159.

Kochansky-Devidé, V., & Slišković, T. (1978). Miocene Congeria from Croatia and Bosnia and Herzegovina. *Rad Jugoslavenske Akademije Znanosti i Umjetnosti*, 1–98.

Kovács, I., Csontos, L., Szabó, Cs., Bali, E., Falus, Gy., Benedek, K., & Zajacz, Z. (2007). Paleogene–early Miocene igneous rocks and geodynamics of the Alpine-Carpathian-Pannonian-Dinaric region: an integrated approach. In *Cenozoic Volcanism in the Mediterranean Area* (ed. L. Beccaluva, G. Bianchini, & M. Wilson). Geological Society of America.

Krajišnik, D., Daković, A., Milić, J., & Marković, M. (2019). Chapter 2 – Zeolites as potential drug carriers. In *Modified Clay and Zeolite Nanocomposite Materials*, pp. 27–55 (ed. M. Mercurio, B. Sarkar, & A. Langella). Elsevier.

Kříbek, B., Knésl, I., Rojík, P., Sýkorová, I., & Martínek, K. (2017). Geochemical history of a Lower Miocene lake, the Cypris Formation, Sokolov Basin, *Czech Republic.* Journal of Paleolimnology, *58*, 169–190.

Krstić, N., Dumurdzanov, N., Jankonić-Golubović, J., Vujnović, L., & Olujić, J. (2001). Interbedded tuff and bentonite in the Neogene lacustrine sediments of the Balkan Peninsula. A review. *Acta Vulcanologica*, *13*.

Laveuf, C., & Cornu, S. (2009). A review on the potentiality of rare earth elements to trace pedogenetic processes. *Geoderma*, *154*, 1–12.

Li, F., Webb, G.E., Algeo, T.J., Kershaw, S., Lu, C., Oehlert, A.M., Gong, Q., Pourmand, A., and Tan, X. (2019). Modern carbonate ooids preserve ambient aqueous REE signatures. *Chemical Geology*, *509*, 163–177.

Li, M.Y.H., & Zhou, M.-F. (2020). The role of clay minerals in formation of the regolith-hosted heavy rare earth element deposits. *American Mineralogist*, *105*, 92–108.

Li, M.Y.H., & Zhou, M.-F. (2023). Physicochemical variation of clay minerals and enrichment of rare earth elements in regolith-hosted deposits: exemplification from the Bankeng Deposit in South China. *Clays and Clay Minerals*, *71*, 362–376.

Liao, Z., Hu, W., Cao, J., Wang, X., Yao, S., Wu, H., & Wan, Y. (2016). Heterogeneous volcanism across the Permian–Triassic Boundary in South China and implications for the Latest Permian Mass Extinction: new evidence from volcanic ash layers in the Lower Yangtze Region. *Journal of Asian Earth Sciences*, *127*, 197–210.

Liu, X., Zhou, F., Chi, R., Feng, J., Ding, Y., & Liu, Q. (2019). Preparation of modified montmorillonite and its application to rare earth adsorption. *Minerals*, *9*, 747.

Liu, X., Tournassat, C., Grangeon, S., Kalinichev, A.G., Takahashi, Y., & Marques Fernandes, M. (2022). Molecular-level understanding of metal ion retention in clay-rich materials. *Nature Reviews Earth & Environment*, *3*, 461–476.

Lukács, R., Harangi, S., Guillong, M., Bachmann, O., Fodor, L., Buret, Y., Dunkl, I., Sliwinski, J., von Quadt, A., Peytcheva, I., & Zimmerer, M. (2018). Early to Mid-Miocene syn-extensional massive silicic volcanism in the Pannonian Basin (East-Central Europe): eruption chronology, correlation potential and geodynamic implications. *Earth-Science Reviews*, *179*, 1–19.

Luo, C., Liang, P., Yang, R., Gao, J., Chen, Q., & Mo, H. (2023). Mineralogical and geochemical constraints on the occurrence forms of REEs in carboniferous karst bauxite, Central Guizhou Province, Southwest China: a case study of Lindai bauxite. *Minerals*, *13*(3).

Macht, F., Eusterhues, K., Pronk, G.J., & Totsche, K.U. (2011). Specific surface area of clay minerals: comparison between atomic force microscopy measurements and bulk-gas (N_2) and -liquid (EGME) adsorption methods. *Applied Clay Science*, *53*, 20–26.

Mandic, O., Pavelić, D., Harzhauser, M., Zupanič, J., Reischenbacher, D., Sachsenhofer, R.F., Tadej, N., & Vranjković, A. (2009). Depositional history of the Miocene Lake Sinj (Dinaride Lake System, Croatia): a long-lived hard-water lake in a pull-apart tectonic setting. *Journal of Paleolimnology*, *41*, 431.

Mandic, O., de Leeuw, A., Vuković, B., Krijgsman, W., Harzhauser, M., & Kuiper, K.F. (2011). Palaeoenvironmental evolution of Lake Gacko (Southern Bosnia and Herzegovina): impact of the Middle Miocene Climatic Optimum on the Dinaride Lake System. *Palaeogeography, Palaeoclimatology, Palaeoecology*, *299*, 475–492.

Mandic, O., de Leeuw, A., Bulić, J., Kuiper, K.F., Krijgsman, W., & Jurišić-Polšak, Z. (2012). Paleogeographic evolution of the Southern Pannonian Basin: $^{40}Ar/^{39}Ar$ age constraints on the Miocene continental series of Northern Croatia. *International Journal of Earth Sciences*, *101*, 1033–1046.

Mandic, O., Rundić, L., Ćorić, S., Pezelj, Đ., Theobalt, D., Sant, K., & Krijgsman, W. (2019a). Age and mode of the middle Miocene marine flooding of the Pannonian Basin—constraints from Central Serbia. *Palaios*, *34*, 71–95.

Mandic, O., Sant, K., Kallanxhi, M.-E., Ćorić, S., Theobalt, D., Grunert, P., de Leeuw, A., & Krijgsman, W. (2019b). Integrated bio-magnetostratigraphy of the Badenian reference section Ugljevik in southern Pannonian Basin-implications for the Paratethys history (middle Miocene, Central Europe). *Global and Planetary Change*, *172*, 374–395.

Mandic, O., Hajek-Tadesse, V., Bakrač, K., Reichenbacher, B., Grizelj, A., & Miknić, M. (2019c). Multiproxy reconstruction of the middle Miocene Požega palaeolake in the Southern Pannonian Basin (NE Croatia) prior to the Badenian transgression of the Central Paratethys Sea. *Palaeogeography, Palaeoclimatology, Palaeoecology*, *516*, 203–219.

Mariner, R.H., & Surdam, R.C. (1970). Alkalinity and formation of zeolites in saline alkaline lakes. *Science*, *170*, 977–980.

Marković, F., Kuiper, K., Ćorić, S., Hajek-Tadesse, V., Kučenjak, M.H., Bakrač, K., Pezelj, Đ., & Kovačić, M. (2021). Middle Miocene marine flooding: new $^{40}Ar/^{39}Ar$ age constraints with integrated biostratigraphy on tuffs from the North Croatian Basin. *Geologia Croatica*, *74*, 237–252.

Martin, J.-M., Høgdahl, O., & Philippot, J.C. (1976). Rare earth element supply to the Ocean. *Journal of Geophysical Research*, *81*, 3119–3124.

Martizzi, P., Chiyonobu, S., & Arato, H. (2020). Sedimentary and geochemical characterization of Middle–Late Miocene formations in the Neogene Tsugaru Basin, Japan by means of DTH27-1 well sediment analysis. *Island Arc*, *29*, e12358.

Matenco, LRadivojević, D. (2012). On the formation and evolution of the Pannonian Basin: derived from the structure of the junction area between the Carpathians and Dinarides. *Tectonics*, *31*(6), https://doi.org/10.1029/2012TC003206.

Matošević, M., Marković, F., Bigunac, D., Suica, S., Krizmanić, K., Perkovic, A., Kovačić, M., & Pavelić, D. (2023). Petrography of the Upper Miocene sandstones from the North Croatian Basin: understanding the genesis of the largest reservoirs in the southwestern part of the Pannonian Basin System. *Geologica Carpathica*, *74*, 155–179.

McHenry, L.J. (2009). Element mobility during zeolitic and argillic alteration of volcanic ash in a closed-basin lacustrine environment: study Olduvai Gorge, Tanzania. *Chemical Geology*, *265*, 540–552.

McLennan, S.M. (1994). Rare earth element geochemistry and the 'tetrad' effect. *Geochimica et Cosmochimica Acta*, *58*, 2025–2033.

McLennan, S.M. (2001). Relationships between the trace element composition of sedimentary rocks and upper continental crust. *Geochemistry, Geophysics, Geosystems*, *2*(12), https://doi.org/10.1029/2000GC000109.

McLennan, S.M., & Ross Taylor, S. (2012). Geology, geochemistry and natural abundances. In *Encyclopedia of Inorganic and Bioinorganic Chemistry*. John Wiley & Sons Ltd.

https://doi.org/10.1017/cmn.2024.21 Published online by Cambridge University Press

Michot, L.J., & Villiéras, F. (2006). *Chapter 12.9 – Surface area and porosity*. In Developments in Clay Science (ed. F. Bergaya, B.K.G. Theng, & G. Lagaly), pp. 965–978. Elsevier.

Moore, D.M., & Reynolds, R.C. (1997). *X-Ray Diffraction and the Identification and Analysis of Clay Minerals* (2nd edn), 400 pp. Oxford University Press.

Nadeau, P.H., Wilson, M.J., McHardy, W.J., & Tait, J.M. (1984). Interstratified clays as fundamental particles. *Science*, *225*, 923–925.

Nagender Nath, B., Bau, M., Ramalingeswara Rao, B., & Rao, C.M. (1997). Trace and rare earth elemental variation in Arabian Sea sediments through a transect across the oxygen minimum zone. *Geochimica et Cosmochimica Acta*, *61*, 2375–2388.

Namayandeh, A., Modabberi, S., & López-Galindo, A. (2020). Trace and rare earth element distribution and mobility during diagenetic alteration of volcanic ash to bentonite in Eastern Iranian bentonite deposits. *Clays and Clay Minerals*, *68*, 50–66.

Németh, K., Martin, U., & Harangi, S. (2001). Miocene phreatomagmatic volcanism at Tihany (Pannonian Basin, Hungary). *Journal of Volcanology and Geothermal Research*, *111*, 111–135.

Nesbitt, H.W. (1979). Mobility and fractionation of rare earth elements during weathering of a granodiorite. *Nature*, *279*, 206–210.

Neubauer, U., Nowack, B., Furrer, G., & Schulin, R. (2000). Heavy metal sorption on clay minerals affected by the siderophore desferrioxamine B. *Environmental Science & Technology*, *34*, 2749–2755.

Ou, X., Chen, Z., Chen, X., Li, X., Wang, J., Ren, T., Chen, H., Feng, L., Wang, Y., Chen, Z., Liang, M., & Gao, P. (2022). Redistribution and chemical speciation of rare earth elements in an ion-adsorption rare earth tailing, Southern China. *Science of the Total Environment*, *821*, 153369.

Pálfy, J., Mundil, R., Renne, P.R., Bernor, R.L., Kordos, L., & Gasparik, M. (2007). U–Pb and $^{40}Ar/^{39}Ar$ dating of the Miocene fossil track site at Ipolytarnóc (Hungary) and its implications. *Earth and Planetary Science Letters*, *258*, 160–174.

Pamić, J., & Hrvatović, H. (2003). Main large thrust structures in the Dinarides – a proposal for their classification. *Nafta*, *54*, 443–464.

Pamić, J., Gušić, I., & Jelaska, V. (1998). Geodynamic evolution of the Central Dinarides. *Tectonophysics*, *297*, 251–268.

Pavelić, D., & Kovačić, M. (1999). Lower Miocene alluvial deposits of the Požeška Mt. (Pannonian Basin, Northern Croatia): cycles, megacycles and tectonic implications. *Geologia Croatica*, *52*, 67–76.

Pavelić, D., & Kovačić, M. (2018). Sedimentology and stratigraphy of the Neogene rift-type North Croatian Basin (Pannonian Basin System, Croatia): a review. *Marine and Petroleum Geology*, *91*, 455–469.

Pavelić, D., Kovačić, M., Miknić, M., Avanić, R., Vrsaljko, D., Bakrac, K., Tisljar, J., Galovic, I., & Bortek, Z. (2003). The evolution of the Miocene environments in the Slavonian Mts. area (northern Croatia). In *Evolution of Depositional Environments from the Palaeozoic to the Quaternary in the Karst Dinarides and the Pannonian Basin*, pp. 17–19. 22nd IAS Meeting of Sedimentology, Opatija-September.

Pavelić, D., Kovačić, M., Tibljaš, D., Galić, I., Marković, F., & Pavičić, I. (2022). The transition from a closed to an open lake in the Pannonian Basin System (Croatia) during the Miocene Climatic Optimum: sedimentological evidence of Early Miocene regional aridity. *Palaeogeography, Palaeoclimatology, Palaeoecology*, *586*, 110786.

Piller, W.E., Harzhauser, M., & Mandic, O. (2007). Miocene Central Paratethys stratigraphy – current status and future directions. *Stratigraphy*, *4*, 151–168.

Pol, A., Barends, T.R.M., Dietl, A., Khadem, A.F., Eygensteyn, J., Jetten, M.S.M., & Op den Camp, H.J.M. (2014). Rare earth metals are essential for methanotrophic life in volcanic mudpots. *Environmental Microbiology*, *16*, 255–264.

Reid-Soukup, D.A., & Ulery, A.L. (2002). Smectites. In *Soil Mineralogy with Environmental Applications*, pp. 467–499. John Wiley & Sons Ltd.

Roeder, D., & Bachmann, G. (1996). Evolution, structure and petroleum geology of the German Molasse Basin. In *Peri-Tethys Memoir 2: Structure and Prospects of Alpine Basins and Forelands* (ed. P. Ziegler & F. Horváth), pp. 263–284. Muséum National d'Histoire Naturelle, Paris, France.

Roetzel, R., de Leeuw, A., Mandic, O., Marton, E., Nehyba, S., Kuiper, K.F., Scholger, R., & Wimmer-Frey, I. (2014). Lower Miocene (upper Burdigalian, Karpatian) volcanic ashfall at the south-eastern margin of the Bohemian massif in Austria-new evidence from $^{40}Ar/^{39}Ar$-dating, palaeomagnetic, geochemical and mineralogical investigations. *Austrian Journal of Earth Sciences*, *107*, 2–22.

Ronov, A.B., & Yaroshevsky, A.A. (1969). Chemical composition of the Earth's crust. In *The Earth's Crust and Upper Mantle*, pp. 37–57. American Geophysical Union (AGU).

Roşu, E., Seghedi, I., Downes, H., Alderton, D.H.M., Szakács, A., Pécskay, Z., Panaiotu, C., Panaiotu, C.E., & Nedelcu, L. (2004). Extension-related Miocene calc-alkaline magmatism in the Apuseni Mountains, Romania: origin of magmas. *Swiss Bulletin of Mineralogy and Petrology*, *84*, 153–172.

Rutherford, D.W., Chiou, C.T., & Eberl, D.D. (1997). Effects of exchanged cation on the microporosity of montmorillonite. *Clays and Clay Minerals*, *45*, 534–543.

Rybár, S., Šarinová, K., Sant, K., Kuiper, K.F., Kováčová, M., Vojtko, R., Reiser, M.K., Fordinál, K., Teodoridis, V., Nováková, P., & Vlček, T. (2019). New $^{40}Ar/^{39}Ar$, fission track and sedimentological data on a middle Miocene tuff occurring in the Vienna Basin: implications for the north-western Central Paratethys region. *Geologica Carpathica*, *70*, 386–404.

Sanders, R.L., Washton, N.M., & Mueller, K.T. (2010). Measurement of the reactive surface area of clay minerals using solid-state NMR studies of a probe molecule. *Journal of Physical Chemistry C*, *114*, 5491–5498.

Šarinová, K., Hudáčková, N., Rybár, S., Jamrich, M., Jourdan, F., Frew, A., Mayers, C., Ruman, A., Subová, V., & Sliva, Ľ. (2021). $^{40}Ar/^{39}Ar$ dating and palaeoenvironments at the boundary of the early-late Badenian (Langhian-Serravallian) in the northwest margin of the Pannonian basin system. *Facies*, *67*, 29.

Šćavničar, S., Krkalo, E., Šćavničar, B., Halle, R., & Tibljaš, D. (1983). Analcime bearing beds in Poljanska. *Rad Jugoslavenske Akademije Znanosti i Umjetnosti*, *404*, 137–169.

Schmid, S.M., Fügenschuh, B., Kissling, E., & Schuster, R. (2004). Tectonic map and overall architecture of the Alpine orogen. *Eclogae Geologicae Helvetiae*, *97*, 93–117.

Schmid, S.M., Bernoulli, D., Fügenschuh, B., Matenco, L., Schefer, S., Schuster, R., Tischler, M., & Ustaszewski, K. (2008). The Alpine-Carpathian-Dinaridic orogenic system: correlation and evolution of tectonic units. *Swiss Journal of Geosciences*, *101*, 139–183.

Schmid, S.M., Fügenschuh, B., Kounov, A., Maţenco, L., Nievergelt, P., Oberhänsli, R., Pleuger, J., Schefer, S., Schuster, R., Tomljenović, B., Ustaszewski, K., & van Hinsbergen, D.J.J. (2020). Tectonic units of the Alpine collision zone between Eastern Alps and western Turkey. *Gondwana Research*, *78*, 308–374.

Schroeder, P.A., Austin, J.C., Thompson, A., & Richter, D.D. (2022). Mineralogical and elemental trends in regolith on historically managed sites in the southeastern United States Piedmont. *Clays and Clay Minerals*, *70*, 539–554.

Schudel, G., Lai, V., Gordon, K., & Weis, D. (2015). Trace element characterization of USGS reference materials by HR-ICP-MS and Q-ICP-MS. *Chemical Geology*, *410*, 223–236.

Seghedi, I. & Downes, H. (2011). Geochemistry and tectonic development of Cenozoic magmatism in the Carpathian–Pannonian region. *Gondwana Research*, *20*, 655–672.

Šegvić, B., Mileusnić, M., Aljinović, D., Vranjković, A., Mandic, O., Pavelić, D., Dragičević, I., & Ferreiro Mählmann, R. (2014). Magmatic provenance and diagenesis of Miocene tuffs from the Dinaride Lake System (the Sinj Basin, Croatia). *European Journal of Mineralogy*, *26*, 83–101.

Šegvić, B., Zanoni, G., & Moscariello, A. (2020). On the origins of eogenetic chlorite in verdine facies sedimentary rocks from the Gabon Basin in West Africa. *Marine and Petroleum Geology*, *112*, 104064.

Šegvić, B., Lukács, R., Mandic, O., Strauss, P., Badurina, L., Guillong, M., & Harzhauser, M. (2023a). U–Pb zircon age and mineralogy of the St Georgen halloysite tuff shed light on the timing of the middle Badenian (mid-Langhian) transgression, ash dispersal and palaeoenvironmental conditions in the southern Vienna Basin, Austria. *Journal of the Geological Society*, *180*.

Šegvić, B., Slovenec, D., & Badurina, L. (2023b). Major and rare earth element mineral chemistry of low-grade assemblages inform dynamics of hydrothermal ocean-floor metamorphism in the Dinaridic Neotethys. *Geological Magazine*, *160*, 444–470.

https://doi.org/10.1017/cmn.2024.21 Published online by Cambridge University Press

Sekine, Y. (1963). On the concept of concentration of ore-forming elements and the relationship of their frequency in the Earth's crust. *International Geology Review*, *5*, 505–515.

Sholkovitz, E.R., Landing, W.M., & Lewis, B.L. (1994). Ocean particle chemistry: the fractionation of rare earth elements between suspended particles and seawater. *Geochimica et Cosmochimica Acta*, *58*, 1567–1579.

Simić, V., Životić, D., & Miladinović, Z. (2021). Towards better valorisation of industrial minerals and rocks in Serbia – case study of industrial clays. *Resources*, *10*, 63.

Sposito, G., Skipper, N.T., Sutton, R., Park, S., Soper, A.K., & Greathouse, J.A. (1999). Surface geochemistry of the clay minerals. *Proceedings of the National Academy of Sciences*, *96*, 3358–3364.

Środoń, J. (1980). Precise identification of illite/smectite interstratifications by X-ray powder diffraction. *Clays and Clay Minerals*, *28*, 401–411.

Środoń, J. (2013). Identification and quantitative analysis of clay minerals. *Developments in Clay Science*, *5*, 25–49.

Stojadinovic, U., Matenco, L., Andriessen, P., Toljić, M., Rundić, L., & Ducea, M. N. (2017). Structure and provenance of Late Cretaceous–Miocene sediments located near the NE Dinarides margin: inferences from kinematics of orogenic building and subsequent extensional collapse. *Tectonophysics*, *710–711*, 184–204.

Suárez, M., Lorenzo, A., García-Vicente, A., Morales, J., García-Rivas, J., & García-Romero, E. (2022). New data on the microporosity of bentonites. *Engineering Geology*, *296*, 106439.

Šujan, M., Rybár, S., Kováč, M., Bielik, M., Majcin, D., Minár, J., Plašienka, D., Nováková, P., & Kotulová, J. (2021). The polyphase rifting and inversion of the Danube Basin revised. *Global and Planetary Change*, *196*, 103375.

Summa, L.L., & Verosub, K.L. (1992). Trace element mobility during early diagenesis of volcanic ash: applications to stratigraphic correlation. *Quaternary International*, *13–14*, 149–157.

Sunarić, O., Glišić, R., Dangić, A., & Milivojević, R. (1976). Baseni, ležišta i pojave mrkog uglja u Bosni i Hercegovini. In *Mineralne Sirovine Bosne i Hercegovine*. Geološki zavod Sarajevo, Sarajevo.

Szabó, C., Harangi, S., & Csontos, L. (1992). Review of Neogene and Quaternary volcanism of the Carpathian-Pannonian region. *Tectonophysics*, *208*, 243–256.

Tanaka, K., & Kawabe, I. (2006). REE abundances in ancient seawater inferred from marine limestone and experimental REE partition coefficients between calcite and aqueous solution. *Geochemical Journal*, *40*, 425–435.

Tari, V. (2002). Evolution of the northern and western Dinarides: a tectonostratigraphic approach. *Continental Collision and the Tectono-Sedimentary Evolution of Forelands*. Copernicus, Göttingen.

Taylor, S.R. & McLennan, S.M. (1995). The geochemical evolution of the continental crust. *Reviews of Geophysics*, *33*, 241–265.

Terakado, Y. & Nakajima, W. (1995). Characteristics of rare-earth elements, Ba, Sr and Rb abundances in natural zeolites. *Geochemical Journal*, *29*, 337–345.

Topp, N.E. (1965). *Chemistry of the Rare-Earth Elements*. Elsevier Applied Science.

Tournassat, C., Bourg, I.C., Steefel, C.I., & Bergaya, F. (2015). *Chapter 1 – Surface properties of clay minerals*. In Developments in Clay Science (ed. C. Tournassat, C.I. Steefel, I.C. Bourg, & F. Bergaya), pp. 5–31. Elsevier.

Trinajstić, N., Brlek, M., Gaynor, S.P., Schindlbeck-Belo, J., Šuica, S., Avanić, R., Kutterolf, S., Wang, K.-L., Lee, H.-Y., Holcová, K., Kopecká, J., Baranyi, V., Hajek-Tadesse, V., Bakrač, K., Brčić, V., Kukoč, D., Milošević, M., Mišur, I. & Lukács, R. (2023). Provenance and depositional environment of Middle Miocene silicic volcaniclastic deposits from Mt. Medvednica (North Croatian Basin, Carpathian-Pannonian Region). *Journal of Volcanology and Geothermal Research*, *443*, 107917. https://doi.org/10.1016/j.jvolgeores.2023.107917

Tütken, T., Vennemann, T.W., Janz, H., & Heizmann, E.P.J. (2006). Palaeoenvironment and palaeoclimate of the Middle Miocene lake in the Steinheim basin, SW Germany: a reconstruction from C, O, and Sr isotopes of fossil remains. *Palaeogeography, Palaeoclimatology, Palaeoecology*, *241*, 457–491.

van Unen, M., Matenco, L., Nader, F.H., Darnault, R., Mandic, O., & Demir, V. (2019). Kinematics of foreland-vergent crustal accretion: inferences from the Dinarides Evolution. *Tectonics*, *38*, 49–76.

Uzarowicz, Ł., Šegvić, B., Michalik, M., & Bylina, P. (2012). The effect of hydrochemical conditions and pH of the environment on phyllosilicate transformations in the weathering zone of pyrite-bearing schists in Wieściszowice (SW Poland). *Clay Minerals*, *47*, 401–417.

Vaitkus, A., Merkys, A., & Gražulis, S. (2021). Validation of the Crystallography Open Database using the Crystallographic Information Framework. *Journal of Applied Crystallography*, *54*, 661–672.

Valsami, E. & Cann, J.R. (1992). Mobility of rare earth elements in zones of intense hydrothermal alteration in the Pindos ophiolite, Greece. *Geological Society, London, Special Publications*, *60*, 219–232.

Vannoorenberghe, M., Acker, T.V., Belza, J., Teetaert, D., Crombé, P., & Vanhaecke, F. (2020). Multi-element LA-ICP-MS analysis of the clay fraction of archaeological pottery in provenance studies: a methodological investigation. *Journal of Analytical Atomic Spectrometry*, *35*, 2686–2696.

Vranjković, A. (2011). Klimatski zapisi u miocenskim slatkovodnim naslagama Sinjskoga bazena [*Records from Miocene freshwater beds of the Sinj Basin*]. Thesis, University of Zagreb, Zagreb, 154 pp.

Willis, S.S., & Johannesson, K.H. (2011). Controls on the geochemistry of rare earth elements in sediments and groundwaters of the Aquia aquifer, Maryland, USA. *Chemical Geology*, *285*, 32–49.

Wu, Z., Chen, Y., Wang, Y., Xu, Y., Lin, Z., Liang, X., & Cheng, H. (2023). Review of rare earth element (REE) adsorption on and desorption from clay minerals: application to formation and mining of ion-adsorption REE deposits. *Ore Geology Reviews*, *157*, 105446.

Xu, L., Zhang, J., Ding, J., Liu, T., Shi, G., Li, X., Dang, W., Cheng, Y., & Guo, R. (2020). Pore structure and fractal characteristics of different shale lithofacies in the Dalong Formation in the Western Area of the Lower Yangtze Platform. *Minerals*, *10*, 72.

Yamamoto, K., Sugisaki, R., & Arai, F. (1986). Chemical aspects of alteration of acidic tuffs and their application to siliceous deposits. *Chemical Geology*, *55*, 61–76.

Yang, M., Liang, X., Ma, L., Huang, J., He, H., & Zhu, J. (2019). Adsorption of REEs on kaolinite and halloysite: a link to the REE distribution on clays in the weathering crust of granite. *Chemical Geology*, *525*, 210–217.

Zachos, J., Pagani, M., Sloan, L., Thomas, E., & Billups, K. (2001). Trends, rhythms, and aberrations in global climate 65 Ma to present. *Science*, *292*, 686–693.

Zhang, Y., Gao, X., & Arthur Chen, C.-T. (2014). Rare earth elements in intertidal sediments of Bohai Bay, China: concentration, fractionation and the influence of sediment texture. *Ecotoxicology and Environmental Safety*, *105*, 72–79.

Zhao, T., Xu, S., & Hao, F. (2023). Differential adsorption of clay minerals: Implications for organic matter enrichment. *Earth-Science Reviews*, *246*, 104598.

Zhou, M.-F., Li, M.Y.H., Wang, Z., Li, X.-C., & Liu, J. (2020). The genesis of regolith-hosted rare earth element and scandium deposits: current understanding and outlook to future prospecting. *Kexue Tongbao/Chinese Science Bulletin*, *65*, 3809–3824.

Zytnick, A.M., Gutenthaler-Tietze, S.M., Aron, A.T., Reitz, Z.L., Phi, M.T., Good, N. M., Petras, D., Daumann, L.J., & Martinez-Gomez, N.C. (2023). Discovery and characterization of the first known biological lanthanide chelator. *bioRxiv*. <https://www.biorxiv.org/content/10.1101/2022.01.19.476857v2> (12 April 2024).

https://doi.org/10.1017/cmn.2024.21 Published online by Cambridge University Press